arXiv:1210.2407v3 [hep-ph] 29 Nov 2012

Exclusive final states in diffractive excitation[*]

Christoffer Flensburg, Gösta Gustafson, and Leif Lönnblad

Dept. of Astronomy and Theoretical Physics, Lund University, Sölvegatan 14A, Lund, Sweden

E-mail: christoffer.flensburg@thep.lu.se, gosta.gustafson@thep.lu.se, leif.lonnblad@thep.lu.se

ABSTRACT: In this paper we describe a formalism for generating exclusive final states in diffractive excitation, based on the optical analogy where diffraction is fully determined by the absorption into inelastic channels. The formalism is based on the Good–Walker formalism for diffractive excitation, and it is assumed that the virtual parton cascades represent the diffractive eigenstates defined by a definite absorption amplitude. We emphasize that, although diffractive excitation is basically a quantum-mechanical phenomenon with strong interference effects, it is possible to calculate the different interfering components to the amplitude in an event generator, add them and thus calculate the reaction cross section for exclusive diffractive final states. The formalism is implemented in the DIPSY event generator, introducing no tunable parameters beyond what has been determined previously in studies of non-diffractive events. Some early results for DIS and proton-proton collisions are presented, and compared to experimental data.

KEYWORDS: Diffraction, Small-x physics, Saturation, Dipole Model, DIS.

Contents

1. Introduction

Although most events in high energy collisions have a continuous distribution of hadrons, events with rapidity gaps are not rare; they contribute of the order 10% both in DIS at HERA [1, 2], and in $p\bar{p}$ collisions at the CERN $Sp\bar{p}S$ collider [3, 4] and the Tevatron [5]. These events have commonly been interpreted as the shadow of absorption into inelastic channels, in analogy with diffraction in optics. In this view diffraction is expected to be a quantum-mechanical phenomenon, to be analyzed at amplitude level, and not directly treatable by semiclassical probabilistic methods.

In the Regge formalism the absorption is represented by cut pomeron or reggeon diagrams. Regge diagrams, cut in between two exchanged pomerons or reggeons, represent elastic scattering, while diffractive excitation originates from triple pomeron diagrams, cut through one of the pomerons [6, 7]. At high energies multi-Regge diagrams, where the relative contributions from cut and uncut diagrams are given by the AGK cutting rules [8], are important. Recent analyses within this formalism include work by Kaidalov and coworkers [9], Ostapchenko [10], the Durham [11, 12], and the Tel Aviv groups [13–15]. These analyses give results for inclusive diffractive cross sections and distributions in $d\sigma/dM_X^2$, but do not give information about details in the diffractive final states. (Ref. [9] makes the extra assumption that a pomeron interacts like a $q\bar{q}$ pair.) A scheme for generation of exclusive diffractive final states is outlined in ref. [16], but as far as we know, no results are presented yet. We note that, in contrast to our approach which is based on amplitudes, in this scheme diffractive events are generated as a semi-classical probabilistic process.

Diffractive excitation has also been described within the Good–Walker formalism [17], where it is the result of differences in absorption probability between different components of the projectile wavefunction. In the Regge approaches mentioned above, this formalism was used only for low mass excitation. It was, however, early proposed by Miettinnen and Pumplin [18], that fluctuations between parton cascades with different absorption probability also can describe excitation to high masses. In QCD a high energy proton is visualized as a virtual cascade, with partons filling the rapidity range between the proton rest frame and the observer. This implies that the proton wavefunction also contains components with high masses $\sim \exp(rapidity\ range)$. In high energy collisions the cascades are determined by the BFKL dynamics, which has a stochastic nature with large fluctuations, and in the dipole formulation these cascades are also eigenstates of the interaction [19]. These fluctuations were studied by Hatta *et al.* [20] in an analysis of diffractive excitation in DIS at very high energies, within the saturated region where $Q^2 < Q_s^2$. This approach to diffractive excitation has also been exploited by the Lund group within the dipole cascade model implemented in the DIPSY Monte Carlo [21, 22], with applications to DIS and pp collisions at present day collider energies. It is the aim of this paper to generalize this approach to calculate amplitudes for transitions to exclusive final states.

In both the triple-Regge and the Good–Walker formalisms the diffractive amplitude is via the optical theorem determined by the inelastic cross section. At high energies inelastic events result from gluon exchange, which causes colour connections between projectile and target, and the diffractive amplitude is represented by the (uncut) perturbative BFKL pomeron formed by a two-gluon ladder. The stochastic nature of the BFKL pomeron is also present in the AGK cutting rules. In ref. [23] it is argued that the triple-pomeron and Good–Walker formalisms only represent different views of the same phenomenon. This idea is also supported by the fact that the bare pomeron in the DIPSY model also reproduces the triple-Regge form for the diffractive excitation cross section [22].

In the "colour reconnection" approach it is assumed that the colour exchange from an initial hard subcollision can be neutralized through the mediation of subsequent soft gluons [24,25]. In this picture the cross section for gap events is determined by a reconnection probability. This can be tuned to fit experimental data, but is in this picture not dynamically fixed by the total inelastic cross section, and the relation to diffraction in optics is not clear.

Of particular interest in analyses of diffractive excitation are the increased effects of saturation at higher energies. In DIS diffractive excitation of the photon has been calculated from elastic scattering of $q\bar{q}$ and $q\bar{q}g$ states. Golec-Biernat and Wüsthoff [26,27] have emphasized that the coupling of a virtual photon is significant to large $q\bar{q}$ dipoles with highly asymmetric energies, but that the coupling to the proton is suppressed for dipoles larger than the saturation scale $R_0 \sim 1/Q_s(x)$. This implies on one hand a suppression of the diffractive cross section, and on the other hand that the interaction is not dominated by soft interaction, but can be treated by perturbative QCD. This argument should also be applicable for diffraction in pp collisions, suggesting that also this can be treated by perturbative methods.

In pp collisions the absorptive cross section is larger than in DIS. In the Good–Walker formalism diffractive excitation is determined by the fluctuations in absorption probability, which become small when the black disk limit is approached. Thus diffraction is dominated by elastic scattering, when the saturation effects become large at higher energy, in particular for small impact parameters. In the Regge formalism these saturation effects are represented by "enhanced diagrams", which interfere destructively and reduce the probability for a rapidity gap. Also in the colour reconnection formalism, the large number of partons participating in the collision tends to fill in a potential gap. In the analysis by Goulianos [28], these saturation effects are described by a "renormalized pomeron flux", which starts to become noticeable in pp collisions around $\sqrt{s} \approx 20$ GeV.

Most of the analyses cited above estimate inclusive distributions in $d\sigma/dM_X^2$ (or $d\sigma/d\eta_{\max}$) or semi-inclusive hard processes. To understand the properties of *exclusive final states* additional information or assumptions are needed. At lower masses, M_X, diffractively excited pions or protons fragment in a string-like manner; an excited pion is similar to an e^+e^--annihilation event [29], while an excited proton has similarities to DIS [30,31]. These observations are in agreement with the model by Donnachie and Landshoff, in which the pomeron is assumed to interact with the quarks in the target like a photon [32].

For higher masses, the limited acceptance of the detectors at the CERN $Sp\bar{p}S$ col-

lider and the Tevatron implies that the experimental data usually do not cover the full phase space, and the experimental knowledge about the properties of high mass diffractive final states is therefore also limited. At the CERN $Sp\bar{p}S$ collider rapidity distributions were measured by the UA5 collaboration [4]. The result was consistent with a $p_\perp$-limited fragmentation, although there was here no experimental information about transverse momenta. Similar results were obtained by the UA4 collaboration [3], which pointed out the similarity between a diffractive system and a non-diffractive pp collision at $\sqrt{s} = M_X$. At the HERA detectors the coverage of the photon fragmentation end is quite good, although an excited proton is mainly outside the acceptance. Here the diffractively excited photon gives higher multiplicity and lower thrust than an e^+e^--annihilation event with the same mass [33].

High $p_\perp$ jets in diffractive states were observed by the UA8 collaboration [34], but the limited acceptance did not allow a detailed study of the diffractive state, *e.g.* of how the recoil was distributed. "Hard diffraction" with high $p_\perp$ jets have later also been observed at the Tevatron [35, 36] and at HERA [37, 38]. Due to the implications for detection of exclusive central Higgs production, the observation of hard central production with two rapidity gaps at the Tevatron, *e.g.* of dijets [39] and e^+e^- pairs [40], has gained special interest.

Hard diffraction has frequently been analyzed within the Ingelman-Schlein formalism [41], assuming that the pomeron interacts as composed of partons, in a way similar to a hadron. The diffractive interaction is expressed in terms of a flux factor $f_{\mathbb{P}p}(x_\mathbb{P})$, describing the probability to find a pomeron with energy fraction $x_\mathbb{P}$ in the proton, times the inelastic interaction between the pomeron and the projectile proton or virtual photon. In this way analyses of HERA data for both hard and soft diffraction have been described by a common set of "pomeron structure functions" $f_{q/g,\mathbb{P}}(\beta)$, which have been fitted to a DGLAP evolution scheme [42]. These analyses indicate a dominant gluonic component in the pomeron. This leads to more complicated final states than the straight strings seen at lower masses, in agreement with the observations in refs. [3] and [33] mentioned above.

This approach is also implemented in several Monte Carlo (MC) event generators used in analyses of experimental data, *e.g.* POMPYT [43], RAPGAP [44], and PYTHIA8 [45]. In these models the result depends on pomeron flux factors and pomeron structure functions, which have to be fitted to data. Here the effects of saturation have to be included in the flux factor, or in "gap survival factors".

The aim of this paper is to present a formalism, in which the cross section for exclusive diffractive final states can be calculated directly based on the dynamical features of small x evolution and saturation. The formalism is an extension of the Lund Dipole Cascade model implemented in the DIPSY MC [46, 47], which is based on BFKL evolution, including essential non-leading effects, and saturation within the cascade evolution. Hence the model is based on perturbative QCD, which might be motivated by Golec-Biernat–Wüsthoff's argument that gluons below the saturation scale Q_s are suppressed at small x. Diffractive excitation is calculated within the Good–Walker formalism with no additional free parameters. Results for inclusive diffractive cross sections have been presented previously [21, 22], the generation of exclusive non-diffractive final states was discussed in ref. [47], and the

model is here extended to describe exclusive final states in diffractive excitation.

We want to emphasize that, although in the optical analogy diffractive excitation is basically a quantum-mechanical phenomenon with strong interference effects, it is in our formalism possible to calculate the different interfering contributions to the amplitude in the DIPSY MC, add them with their proper signs, and thus calculate the reaction cross section. This distinguishes our formulation from other approaches, in which final states are generated as a semi-classical probabilistic process.

The outline of the paper is as follows: In section 2 we review shortly the eikonal approximation and the Good–Walker formalism. The dipole cascade model is described in section 3, and in section 4 we discuss how this model can be extended to describe exclusive final states in diffractive excitation. In section 5 we discuss the implementation in the DIPSY event generator, and in section 6 we present some early results. Some possible future developments are discussed in section 7, followed by our conclusions in section 8.

2. Diffractive excitation in the Good–Walker picture

2.1 The Good–Walker formalism

In the Good–Walker formalism [17], diffraction in hadronic collisions is analogous to diffraction in optics, and a result of absorption and unitarity. Unitarity constraints and saturation are most easily treated by the eikonal formalism in impact parameter space.

Assume that the elastic scattering is driven by absorption into a number of inelastic states n, with Born amplitudes $\sqrt{2f_n}$. In the eikonal approximation [48] the absorption probability, P_{abs}, is given by the inelastic cross section

$$P_{\mathrm{abs}} = d\sigma_{\mathrm{inel}}/d^2b = 1 - e^{-2F}, \text{ where } F \equiv \sum f_n. \tag{2.1}$$

Thus the probability for the projectile not to be absorbed into any of the inelastic states is given by e^{-2F}.

For a structureless projectile unitarity then gives the S-matrix

$$S = e^{-F} = e^{-\sum f_n}. \tag{2.2}$$

Thus the amplitude for elastic scattering is given by

$$T = 1 - S = 1 - e^{-F}, \tag{2.3}$$

which satisfies the optical theorem $T = \frac{1}{2}(T^2 + P_{\mathrm{abs}})$. Note that we have here defined the amplitude T without the conventional factor i, so that T becomes real. The elastic cross section is given by $d\sigma_{\mathrm{el}}/d^2b = T^2$, and adding the inelastic cross section, the total cross section is given by $d\sigma_{\mathrm{tot}}/d^2b = 2(1 - e^{-F}) = 2T$.

If the projectile has an *internal structure*, it can be excited in a diffractive scattering event. This implies that the mass eigenstates Ψ_k (asymptotic incoming and outgoing states) can differ from the diffractive eigenstates, *i.e.* eigenstates to the S-matrix. We denote the diffractive eigenstates Φ_i, with eigenvalues given by $S\Phi_i = e^{-F_i}\Phi_i$. They can be absorbed

with probability $1 - e^{-2F_i}$, and have elastic scattering amplitudes $\langle\Phi_i|T|\Phi_j\rangle = \delta_{ij}T_i$, with $T_i = 1 - e^{-F_i}$.

The diffractive eigenstates can be written as linear combinations of the mass eigenstates,

$$\Phi_i = \sum_k c_{ik}\Psi_k, \tag{2.4}$$

where c_{ik} is a unitary matrix (thus $\Psi_k = \sum c_{ki}^\dagger\Phi_i$), and the incoming state is given by $\Psi_{\text{in}} = \Psi_0$. The elastic amplitude is then given by the average over the diffractive eigenstates:

$$\langle\Psi_0|T|\Psi_0\rangle = \sum |c_{i0}|^2 T_i = \langle T\rangle, \tag{2.5}$$

with the elastic cross section

$$d\sigma_{\text{el}}/d^2b = \left(\sum |c_{i0}|^2 T_i\right)^2 = \langle T\rangle^2. \tag{2.6}$$

The amplitude for diffractive transition to the mass eigenstate Ψ_k becomes

$$\langle\Psi_k|T|\Psi_0\rangle = \sum_i c_{ki}^\dagger T_i c_{i0}, \tag{2.7}$$

which gives a total diffractive cross section (including elastic scattering)

$$d\sigma_{\text{diff}}/d^2b = \sum_k \langle\Psi_0|T|\Psi_k\rangle\langle\Psi_k|T|\Psi_0\rangle = \langle T^2\rangle. \tag{2.8}$$

Subtracting the elastic scattering we find the cross section for diffractive excitation

$$d\sigma_{\text{diff ex}}/d^2b = d\sigma_{\text{diff}}/d^2b - d\sigma_{\text{el}}/d^2b = \langle T^2\rangle - \langle T\rangle^2 \equiv V_T, \tag{2.9}$$

which thus is determined by the fluctuations in the scattering process.

2.2 Diffractive eigenstates

The basic assumption in our earlier analyses of diffractive excitation in refs. [21, 22], is that the diffractive eigenstates correspond to parton cascades, which can come on shell through interaction with the target. As mentioned in the introduction, this was also the assumption in the early work by Miettinen and Pumplin [18], and a similar approach has been used by Hatta *et al.* [20]. This means that the factors c_{i0} in eq. (2.4) are given by the evolution of the virtual cascade. The process is illustrated in fig. 1. Fig. 1a shows the virtual cascade before the collision, and fig. 1b illustrates an inelastic interaction, where gluon exchange gives a colour connection between the projectile and the target. This implies that the beam is absorbed with probability $1 - e^{-2F_i}$. In this and the following figures, solid lines represent real emissions present in the final state, while a dashed line corresponds to a virtual emission, which did not come on shell via the interaction with the target, and therefore is reabsorbed in the cascade. Fig. 1c shows an elastic interaction. Via the optical theorem the elastic amplitude is given by the inelastic cross section, represented by the square of the diagram in fig. 1b, which corresponds to the exchange of two gluons. Note that the elastic amplitude in eq. (2.5) is the result of *coherent* interaction of all partons in

Virtual cascade	Inelastic int.	Elastic scatt.	Diffractive ex.
a	b	c	d
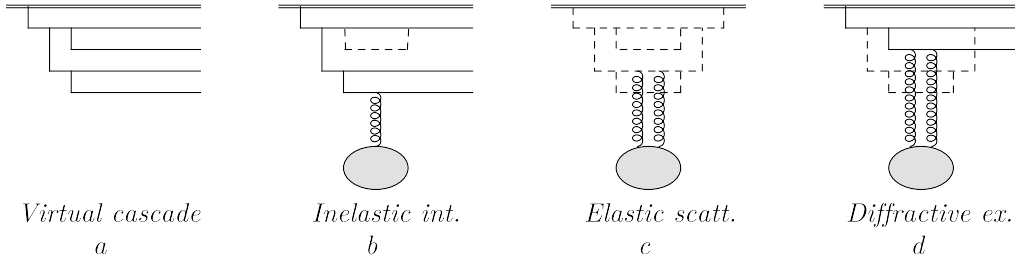
Figure 1: (a) An example of a parton (or dipole) cascade evolved in rapidity. (b) The exchange of a gluon gives rise to an inelastic interaction. (c) Elastic scattering is obtained from coherent scattering of different partons in different cascades, via the exchange of two gluons. (d) Diffractive excitation is obtained when the result of the two-gluon exchange does not correspond to the coherent initial proton state. Dashed lines indicate virtual emissions, which are not present in the final state.

all possible cascades. Fig. 1d, finally, shows the contribution to the scattered beam, which is orthogonal to the incoming state. This corresponds to diffractive excitation, with the amplitude given by eq. (2.7). The lines can symbolise gluons in a traditional cascade, or dipoles in a dipole cascade. When the diagram in fig. 1d is squared, it is consistent with Mueller's triple Regge formalism [6].

3. The dipole cascade model

3.1 Mueller's dipole model

Mueller's dipole cascade model [49–51] is a formulation of LL BFKL evolution in transverse coordinate space. Gluon radiation from the colour charge in a parent quark or gluon is screened by the accompanying anticharge in the colour dipole. This suppresses emissions at large transverse separation, which corresponds to the suppression of small $k_\perp$ in BFKL. For a dipole with charges in transverse points $\mathbf{x}$ and $\mathbf{y}$, the probability per unit rapidity (Y) for emission of a gluon at transverse position $\mathbf{z}$ is given by

$$\frac{d\mathcal{P}}{dY} = \frac{\bar{\alpha}}{2\pi} d^2\mathbf{z} \frac{(\mathbf{x} - \mathbf{y})^2}{(\mathbf{x} - \mathbf{z})^2(\mathbf{z} - \mathbf{y})^2}, \quad \text{with } \bar{\alpha} = \frac{N_c \alpha_s}{\pi}. \tag{3.1}$$

As shown in fig. 2 the dipole is split into two dipoles, which (in the large N_c limit) emit new gluons independently. The result is a cascade, giving a dipole chain where the number of dipoles grows exponentially with Y.

When two cascades collide, a pair of dipoles with coordinates $(\mathbf{x}_i, \mathbf{y}_i)$ and $(\mathbf{x}_j, \mathbf{y}_j)$, in the projectile and target respectively, can interact via gluon exchange with the probability $2f_{ij}$, where

$$f_{ij} = f(\mathbf{x}_i, \mathbf{y}_i | \mathbf{x}_j, \mathbf{y}_j) = \frac{\alpha_s^2}{8} \left[\log\left(\frac{(\mathbf{x}_i - \mathbf{y}_j)^2(\mathbf{y}_i - \mathbf{x}_j)^2}{(\mathbf{x}_i - \mathbf{x}_j)^2(\mathbf{y}_i - \mathbf{y}_j)^2} \right) \right]^2. \tag{3.2}$$

We note here that the interaction probability goes to zero for a small dipole. This implies that the singularity in the production probability for small dipoles in eq. (3.1) does not give infinite cross sections. We note also that gluon exchange means exchange of colour
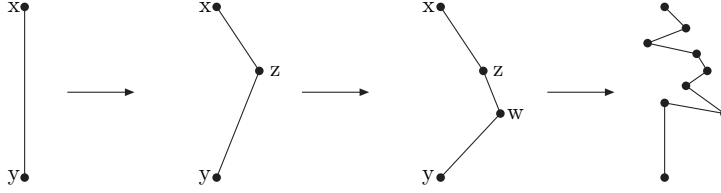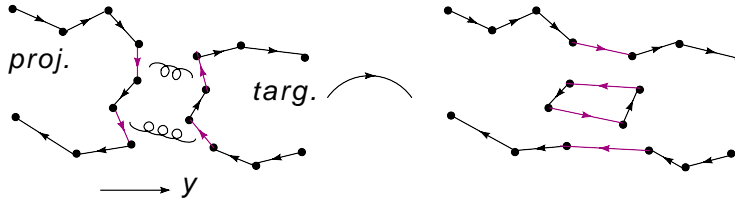
Figure 2: Gluon emission splits the dipole into two dipoles. Repeated emissions give a cascade, which produces a chain of dipoles.
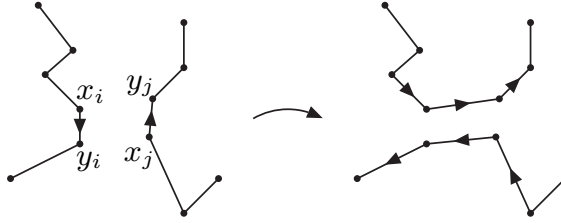
Figure 3: An interaction between a dipole in the projectile and another in the target due to gluon exchange gives a recoupling of the dipole chains.

Figure 4: Double interaction results in a dipole loop, corresponding to a pomeron loop.

between the two cascades. This implies a reconnection of the dipole chains, as shown in fig. 3, and the formation of dipole chains connecting the projectile and target remnants.

In Mueller's model the constraints from unitarity are satisfied using the eikonal formalism. When more than one pair of dipoles interact, colour loops are formed, as shown in fig. 4.

3.2 The Lund dipole cascade model DIPSY

It is well known that non-leading effects are very important in BFKL evolution. Another problem is that Mueller's model does not include pomeron loops within the cascade evolution. The Lund model [46, 47, 52, 53] is a generalization of Mueller's model, which also includes NLL BFKL effects, nonlinear (colour-suppressed) effects in the evolution, and confinement effects.

a) Beyond LL BFKL

The NLL corrections to BFKL evolution have three major sources [54]:
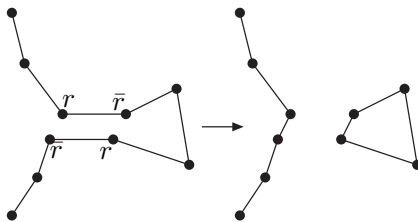
Figure 5: Two dipoles with the same colour form a colour octet, which may be better approximated by dipoles formed by the closet colour-anticolour pairs. This implies a recoupling of the dipole chains, which favours the formation of small dipoles. Thus the number of dipoles resolved by a probe with given resolution Q^2 is reduced.

Non-singular terms in the splitting function: These terms suppress large z-values in the individual parton branchings. Most of this effect is taken care of by including energy-momentum conservation. This is effectively taken into account by associating a dipole with transverse size r with a transverse momentum $k_\perp = 1/r$, and demanding conservation of the light-cone momentum p_+ in every step in the evolution. This gives an effective cutoff for small dipoles.

Projectile-target symmetry: A parton chain should look the same if generated from the target end as from the projectile end. The corresponding corrections are also called energy scale terms, and are essentially equivalent to the so called consistency constraint [55]. This effect is taken into account by conservation of the negative light-cone momentum components, p_-.

The running coupling: Following ref. [56], the scale in the running coupling is taken as the largest transverse momentum in the vertex.

b) Nonlinear effects in the evolution

As mentioned above, multiple interactions produce loops of dipole chains corresponding to pomeron loops. Mueller's model includes all loops cut in the particular Lorentz frame used for the analysis, but not loops contained within the evolution of the individual projectile and target cascades. As for dipole scattering the probability for such loops is given by α_s, and therefore formally colour suppressed compared to dipole splitting, which is proportional to $\bar{\alpha} = N_c \alpha_s / \pi$. These loops are therefore related to the probability that two dipoles have the same colour. Two dipoles with the same colour form a quadrupole field. Such a field may be better approximated by two dipoles formed by the closest colour–anticolour charges. This corresponds to a recoupling of the colour dipole chains. The process is illustrated in Fig. 5, and we call it a dipole "swing". With a weight for the swing which favours small dipoles, we obtain an almost frame independent result. The number of dipoles in the cascade is not reduced, and the saturation effect is a consequence of the smaller interaction probability for the smaller dipoles. Thus the number of dipoles (or gluons) resolved by a probe with a given resolution Q^2, is reduced. In this way the swing also generates effectively $2 \rightarrow 1$, or in some cases a $2 \rightarrow 0$, transitions.

c) Confinement

As mentioned earlier, saturation effects imply that the cascade evolution is dominated by relatively small dipoles. However, although suppressed, the rare large dipoles generated in a purely perturbative evolution with massless gluons give non-negligible effects, and eventually Froissart's bound will be violated [57]. Therefore confinement is also important, and is taken into account by giving the gluon an effective mass.

3.3 Inclusive cross sections and non-diffractive final states

The Lund cascade model is implemented in a Monte Carlo event generator called DIPSY, with applications to collisions between electrons, protons, and nuclei. An incoming virtual photon is here treated as a $q\bar{q}$ pair, with an initial state wavefunction determined by QED. For an incoming proton we make an ansatz in form of an equilateral triangle of dipoles, but after evolution the result is rather insensitive to the exact form of the initial state.

The model reproduces well the inclusive total and elastic cross sections in pp collisions and DIS, as described in ref. [53]. Diffractive cross sections are reproduced within the Good–Walker formalism [22]. It should, however, here be noted that when the nonlinear effects from saturation are switched off, the result agrees with the triple-pomeron formula for a bare pomeron with intercept $\alpha(0) = 1.21$ and an approximately constant triple-pomeron coupling $g_{3P} = 0.3\,\mathrm{GeV}^{-1}$. This result is a consequence of the common underlying assumption, with diffraction as the shadow of absorption.

The model is also generalized to describe the properties of exclusive non-diffractive final states [47]. We here note that BFKL evolution properly reproduces inclusive observables. For exclusive final states it is necessary to take into account colour coherence and angular ordering, as well as soft radiation, related to the $z = 1$ singularity in the gluon splitting function. These effects are taken into account in the CCFM formalism [58,59], which also reproduces the BFKL result for inclusive cross sections.

An essential point is here the fact that the softer emissions in the CCFM formalism can be resummed, and the total cross section, as well as the structure of the final states, are fully determined by the "$k_\perp$-changing" gluons. We denote the real emitted gluons in a ladder q_i and the virtual links k_i, and momentum conservation then implies $\mathbf{k}_{\perp i-1} = \mathbf{k}_{\perp i} + \mathbf{q}_{\perp i}$. For $k_\perp$-changing emissions $k_{\perp i}$ is either much larger or much smaller than $k_{\perp i-1}$. This also means that $q_{\perp i} \approx \max(k_{\perp i}, k_{\perp i-1})$. These emissions are called "primary gluons" in ref. [60], and "backbone gluons" in ref. [61], and the weight for such a backbone chain is given by

$$\text{weight} = \prod \bar{\alpha}\frac{dq_{\perp i}^2}{q_{\perp i}^2}dy_i. \tag{3.3}$$

As discussed in ref. [62], this feature also gives a dynamical cutoff for small $q_\perp$, which grows slowly with energy, and gives a dynamical description of the cutoff for hard subcollisions needed in event generators like PYTHIA [45] or Herwig [63].

To generate the inelastic final states, we thus have to go through the following steps:

- Generate two dipole cascades for the projectile and the target.

- Determine which dipoles in the projectile and target become colour connected via gluon exchange.

- Extract the backbone chains from the cascades, and remove virtual branches, which cannot come on shell by the interaction.

- Add softer emissions as final state radiation, with appropriate Sudakov form factors.

- Hadronize the gluonic chains.

The results from MC simulations, presented in ref. [47], are able to give a fair reproduction of data for minimum bias and underlying events from LHC and the Tevatron, remembering that this implementation does not include matrix element corrections for hard scattering or contributions from quarks.

4. Exclusive final states in diffractive excitation

4.1 Basic formalism

We will now discuss how to describe exclusive states in diffractive excitation, within the dipole cascade model and the Good–Walker formalism. As discussed in sec. 2.2, the partonic cascades are interpreted as the diffractive eigenstates. Thus the unitary matrix c_{ik} in eq. (2.4) is represented by a unitary operator, describing the cascade evolution. The cascade is absorbed with probability $1 - e^{-2F}$, and via the optical theorem this gives an elastic scattering amplitude $T = 1 - e^{-F}$. The hermitian conjugate matrix, $c_{ki}^\dagger$, in the amplitude for diffractive transition to another mass eigenstate in eq. (2.7), represents an evolution backwards in rapidity, which can reabsorb some of the emitted partons. As cascades with more partons generally are absorbed with higher probability, this backward evolution does not always give the original proton back, but a different partonic system, interpreted as a possible mass eigenstate.

The evolution in rapidity may also be interpreted as an evolution in time, from an incoming state at $t = -\infty$ to the cascade present just before the collision at time $t = 0$. Thus the states at $t = -\infty$ correspond to the mass eigenstates Ψ_k in sec. 2.1 (we include the possibility that this state does not correspond to the ground state Ψ_0), while the evolved states at time $t = -\delta$ correspond to the diffractive eigenstates Φ_i. As the possible cascades are not a discrete set, we describe the cascade evolution by a unitary operator $U(-\delta, -\infty)$, replacing the unitary matrix c_{ik} in eq. (2.4). The interaction of the cascades with the target is described by a diagonal operator T, which corresponds to an evolution operator $U(+\delta, -\delta) \equiv U_{\text{int}} = \mathbb{I} - T$ (where $\mathbb{I}$ denotes the unit matrix). The transformation back to mass eigenstates, obtained by the inverse of the cascade evolution operator, can then be interpreted as describing the evolution from time $t = +\delta$ to $t = \infty$, $U(+\infty, +\delta) = U(-\delta, -\infty)^{-1} = U(-\delta, -\infty)^\dagger$. Thus the total S-matrix is given by

$$S = U(+\infty, +\delta)U(+\delta, -\delta)U(-\delta, -\infty) = U(-\delta, -\infty)^{-1}U_{\text{int}}U(-\delta, -\infty), \qquad (4.1)$$

with the diffractive final state given by

$$\Psi_{\text{out}} = S\Psi_{\text{in}}. \tag{4.2}$$

In order to simplify the subsequent equations, we here expressed the relations in terms of the S-matrix, instead of the transition amplitude T. Note that as the diffractive scattering is the shadow of absorption, this operator in not unitary. In section 7.4 an extended formalism is discussed, in which the non-diffractive states are included, and the S-matrix is a unitary operator.

In order to illustrate the essential features in diffractive excitation, we first study some simple toy models. The results will help understanding the more realistic gluon cascades discussed in the later subsections. In the toy models in sec. 4.2, and in the continuous cascade in sec. 4.3, the gluons are assumed to interact individually, with no effects of screening from neighbouring gluons. Such screening effects are taken into account in the dipole cascade discussed in sec. 4.4. We will here also assume that the cascade only includes gluon emission, and that effects of saturation from gluons joining (sometimes referred to as gluon recombination) can be neglected. Such effects are discussed in secs. 5 and 7.2.

4.2 Toy models
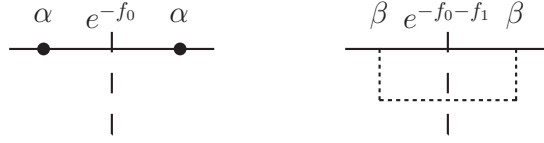
4.2.1 A two-particle system

We first study the simple case of a particle, the valence particle, which can emit a single gluon at a fixed point in phase space. (This example is also directly analogous to the 2-channel Good–Walker treatment of low mass excitation in the work by the Tel Aviv or Durham groups.) The state with no emission and only the original valence particle is denoted $|1,0\rangle$, and the state including the emitted gluon is denoted $|1,1\rangle$. Thus the numbers indicate whether the two particles are present (1) or absent (0). At asymptotic times $t = \pm\infty$ these states are also mass eigenstates, $|1,0\rangle_{\pm\infty}$ and $|1,1\rangle_{\pm\infty}$ respectively. During the evolution up to the collision, the particle can emit a gluon. This is described by the unitary evolution operator $U(-\delta, -\infty)$, which contains a $|1,0\rangle \to |1,1\rangle$ transition. In the $(|1,0\rangle, |1,1\rangle)$ space it can be described by a unitary matrix (we choose phases such that U is real):

$$U(-\delta, -\infty) = \begin{pmatrix} \alpha & -\beta \\ \beta & \alpha \end{pmatrix}, \qquad \alpha^2 + \beta^2 = 1. \tag{4.3}$$

Thus β^2 gives the probability for gluon emission, and α^2 the probability for no emission.

In the collision, which takes place in a short time interval $(-\delta, +\delta)$, we assume that the valence particle and the gluon can be absorbed with probabilities $1 - e^{-2f_0}$ and $1 - e^{-2f_1}$ respectively. In this interaction the beam particle becomes colour-conected to the target, and thus absorbed from the incoming beam. This implies that the states $|1,0\rangle$ and $|1,1\rangle$ have probabilities e^{-2f_0} and $e^{-2(f_0+f_1)}$ *not* to be absorbed. In accordance with the optical theorem, the evolution operator describing the evolution of the diffractive eigenstates during the collision, is given by (*cf* eq. (2.2)):

$$U_{\text{int}} = U(+\delta, -\delta) = \begin{pmatrix} e^{-f_0} & 0 \\ 0 & e^{-f_0-f_1} \end{pmatrix}. \tag{4.4}$$

Figure 6: The diagrams for elastic scattering in a two particle system. In this and subsequent figures a dashed line represents a virtual emission, which is reabsorbed by its parent. A dot represents a possible emission or absorption, which did not occur. The long dashed line indicates the interaction with the target, with the value for U_{int} indicated.

Finally the system evolves from time $+\delta$ to $+\infty$, described by the hermitian conjugate of the unitary matrix $U(-\delta, -\infty)$:

$$U(+\infty, +\delta) = U^{\dagger}(-\delta, -\infty) = \begin{pmatrix} \alpha & \beta \\ -\beta & \alpha \end{pmatrix} \tag{4.5}$$

The S-matrix for the diffractive states is thus given by

$$S = U(+\infty, +\delta)U_{\text{int}}U(-\delta, -\infty) =$$
$$\begin{pmatrix} e^{-f_0}(\alpha^2 + \beta^2\, e^{-f_1}), & -\alpha\beta\, e^{-f_0}(1 - e^{-f_1}) \\ -\alpha\beta\, e^{-f_0}(1 - e^{-f_1}), & e^{-f_0}(\beta^2 + \alpha^2\, e^{-f_1}) \end{pmatrix}. \tag{4.6}$$

The scattering matrix is given by $T = \mathbb{I} - S$, and from the above expression we can read off the scattering amplitudes for an incoming single valence particle. Thus the amplitudes for elastic scattering and diffractive excitation can be written as (recalling that $\alpha^2 + \beta^2 = 1$)

Elastic scattering : $\; T(|1,0\rangle \to |1,0\rangle) = 1 - S_{11} = \alpha^2(1 - e^{-f_0}) + \beta^2(1 - e^{-f_0 - f_1})$ (4.7)

Diffractive excit. : $\; T(|1,0\rangle \to |1,1\rangle) = -S_{21} = \alpha\beta\, e^{-f_0}(1 - e^{-f_1}).$ (4.8)

We note here in particular, that these results agree with the expressions in eqs. (2.6, 2.9), for the case with $c_{ik} = U(-\delta, -\infty)$ given by eq. (4.3) and $T_i = 1 - (U_{\text{int}})_{ii}$ (no summation) given by eq. (4.4).

It will be helpful to represent the different contributions to the amplitudes by associated diagrams. Thus the elastic amplitude is interpreted as the sum of the two diagrams in fig. 6. In the first diagram no gluon is emitted before the collision (weight α), followed by the weight for no absorption of the valence particle (weight e^{-f_0}), and finally no emission is allowed after the interaction (weight α). In the second diagram a virtual gluon is emitted (weight β), followed by the weight for no absorption of the two-particle system (weight $e^{-f_0 - f_1}$), and finally the virtual gluon has to be reabsorbed by the valence particle (weight β).

In the same way the amplitude for diffractive excitation is represented by the diagrams in fig. 7. Here the emitted gluon appears as a real particle in the final state. In the first diagram the gluon is emitted before interaction with weight β, then the system avoids absorption by the target with weight $e^{-f_0 - f_1}$, and finally the gluon also avoids reabsorption
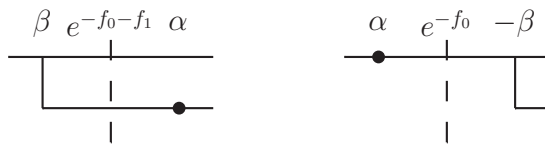
Figure 7: The diagrams for diffractive excitation in a two particle system.

by its parent with weight α. In the second diagram the gluon avoids emission before interaction with weight α, the system is not absorbed by the target with weight e^{-f_0}, and finally the gluon is emitted after the interaction with weight $(-\beta)$. This possibility is a consequence of the unitarity of the evolution operator $U(-\delta, -\infty)$ in eq. (4.3), and the minus sign comes because it is now emitted by $U^\dagger$ and not by U. The two contributions interfere destructively, which gives the factor $(1 - e^{-f_1})$, which also can be interpreted as the amplitude for elastic scattering of the emitted gluon.

This simple example illustrates two essential features of the amplitudes for exclusive states in diffractive excitation:

1. *Fluctuations* in the scattering process are necessary for diffractive excitation, as seen in eq. (2.9). In this toy model the probability for gluon emission is equal to β^2, so the average number of emitted gluons hitting the target is $\langle n \rangle = \beta^2 \cdot 1$, and the variance is $\langle n^2 \rangle - \langle n \rangle^2 = \beta^2 \cdot 1^2 - (\beta^2 \cdot 1)^2 = \alpha^2 \beta^2$. Thus the factor $\alpha\beta$ in the amplitude in eq. (4.8) (to be squared in the cross section) describes the fluctuations in the emission process. The last factor is the difference between the interaction amplitudes of the states with and without emission, and eq. (4.8) shows that diffractive excitation requires fluctuations between different cascades with different interaction amplitudes. We also see that diffractive excitation vanishes in the black disk limit, where f_0 and f_1 become very large, and diffractive scattering becomes purely elastic.

2. Diffraction is fundamentally a quantum mechanical process, where *interference* is important. The two contributions in fig. 6 or 7 have to be added in the amplitude, and not in the cross section.

It should also be noted that the time t can be replaced by any variable, which parametrizes the evolution between the incoming mass eigenstates and the eigenstates for the interaction. A BFKL based cascade would use the rapidity y, while a DGLAP cascade would prefer the transverse momentum $k_\perp$. We will here keep the notation t, and change to y in sec. 4.4, where we will apply the model in DIPSY.

4.2.2 Cascade with two possible emissions

We now study a system in which two different gluons can be emitted. The gluons are denoted 1 and 2, and there are then four different states, with one, two or three particles:

$$|100\rangle, \qquad |110\rangle, \qquad |101\rangle, \qquad |111\rangle. \tag{4.9}$$

The two numbers are here occupation numbers for the three possible particle states.

We first study a sequential cascade, where the first gluon can be emitted from the valence particle, and the second gluon can be emitted from the first one. Thus the emissions are assumed to be ordered in the evolution variable, and the second gluon can only be emitted if the first one already is present. Note that we here do not consider the possibility of a gluon is emitted from one parton and then reabsorbed by another. Such recombination effects beyond the large N_c limit are discussed in secs. 5 and 7.2.

The evolution operator has now two components: the first, U_1, allows the first gluon to be emitted or absorbed by the valence particle, and the second, U_2, allows the second gluon to be emitted or reabsorbed by gluon 1. In the basis in eq. (4.9), these operators can be written

$$U = U_2 U_1, \quad \text{where} \quad U_1 = \begin{pmatrix} \alpha_1 & -\beta_1 & 0 & 0 \\ \beta_1 & \alpha_1 & 0 & 0 \\ 0 & 0 & \alpha_1 & -\beta_1 \\ 0 & 0 & \beta_1 & \alpha_1 \end{pmatrix}, \quad U_2 = \begin{pmatrix} 1 & 0 & 0 & 0 \\ 0 & \alpha_2 & 0 & -\beta_2 \\ 0 & 0 & 1 & 0 \\ 0 & \beta_2 & 0 & \alpha_2 \end{pmatrix}.$$

Thus the first gluon can be emitted with probability β_1^2, and the second with probability β_2^2, once the first is present. This asymmetry also implies that the two matrices U_1 and U_2 do not commute.

The three particles have absorption probabilities $1 - e^{-2f_0}$, $1 - e^{-2f_1}$, and $1 - e^{-2f_2}$ respectively. The evolution operator describing the interaction with the target is then given by

$$U_{\text{int}} = \begin{pmatrix} e^{-f_0} & 0 & 0 & 0 \\ 0 & e^{-f_0-f_1} & 0 & 0 \\ 0 & 0 & e^{-f_0-f_2} & 0 \\ 0 & 0 & 0 & e^{-f_0-f_1-f_2} \end{pmatrix}. \tag{4.10}$$

As in the earlier example, the evolution after the interaction is given by the inverse of $U_2 U_1$. Thus the projection on diffractive states of the S-matrix is

$$S = U_1^\dagger U_2^\dagger U_{\text{int}} U_2 U_1. \tag{4.11}$$

Multiplying the matrices given above, and looking at the first column in the matrix $T = \mathbb{I} - S$, we get the amplitudes relevant for an incoming single valence particle:

$$\begin{aligned} T_{\text{el}} = T(|100\rangle \to |100\rangle) &= \alpha_1^2(1 - e^{-f_0}) + \beta_1^2\alpha_2^2(1 - e^{-f_0-f_1}) \\ &\quad + \beta_1^2\beta_2^2(1 - e^{-f_0-f_1-f_2}) \end{aligned} \tag{4.12}$$

$$T(|100\rangle \to |110\rangle) = e^{-f_0}\alpha_1\beta_1[\alpha_2^2(1 - e^{-f_1}) + \beta_2^2(1 - e^{-f_1-f_2})] \tag{4.13}$$

$$T(|100\rangle \to |101\rangle) = e^{-f_0}\beta_1^2 e^{-f_1}\alpha_2\beta_2(1 - e^{-f_2}) \tag{4.14}$$

$$T(|100\rangle \to |111\rangle) = e^{-f_0}\alpha_1\beta_1 e^{-f_1}\alpha_2\beta_2(1 - e^{-f_2}). \tag{4.15}$$

As in the previous example, these results can also be obtained from a sum of diagrams, as illustrated in figs. 8 – 11. In these diagrams the emission before, or the absorption after, the interaction gives a factor β, while an emission after interaction gives $-\beta$. The absence of a possible emission or reabsorption gives a factor α. The interaction with the target
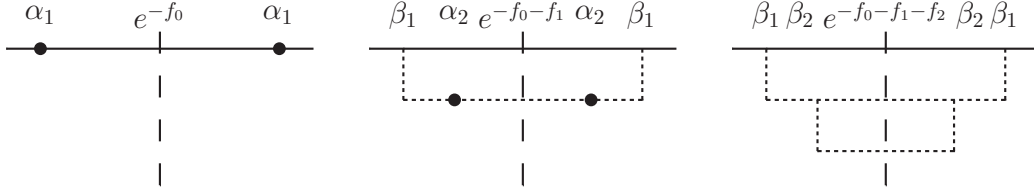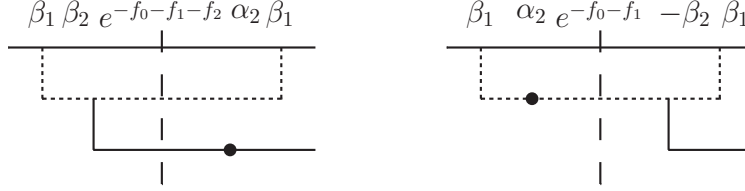
Figure 8: The diagrams for elastic scattering ($|100\rangle \to |100\rangle$) in an ordered three gluon system.
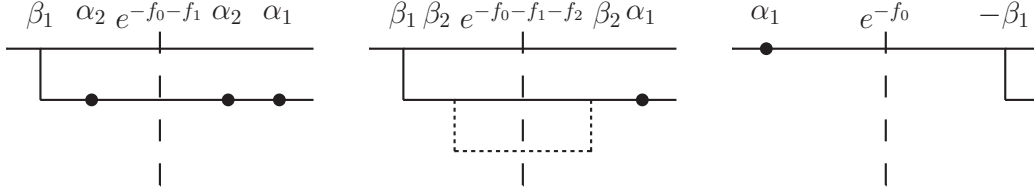
Figure 9: The diagrams for diffractive excitation of the first emission ($|100\rangle \to |110\rangle$) in an ordered three gluon system.

Figure 10: The diagrams for diffractive excitation of the second emission ($|100\rangle \to |101\rangle$) in an ordered three gluon system.

gives a factor e^{-F}, where $F = \sum f_i$, with the sum running over the gluons present at the interaction. The sum of the contributions from the relevant diagrams give the S-matrix elements corresponding to the amplitudes in eqs. (4.12 – 4.15).

In case of two gluons, which can be *independently* emitted from the valence quark, the excited state $|110\rangle$, with a single emission, can be created through the four diagrams in fig. 12, which add up to

$$T(|100\rangle \to |110\rangle) = e^{-f_0}\alpha_1\beta_1(1 - e^{-f_1})(\alpha_2^2 + \beta_2^2 e^{-f_2}) \qquad (4.16)$$

The transition to state $|111\rangle$, with both gluons emitted, would in this case also have four contributions, as shown in fig. 13. The result would then be
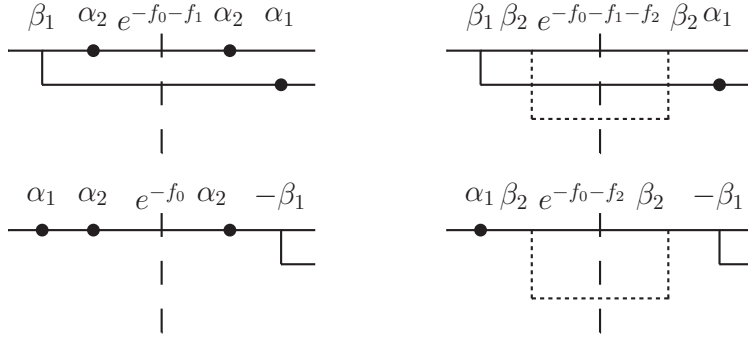
$$T(|000\rangle \to |111\rangle) = e^{-f_0}\alpha_1\beta_1\alpha_2\beta_2(1 - e^{-f_1})(1 - e^{-f_2}). \qquad (4.17)$$

4.2.3 Interpretation

The results in eqs. (4.7, 4.8) and (4.12–4.17) can be represented by a few rules, which in sec. 4.3 and Appendix A are shown to hold also for a general cascade.
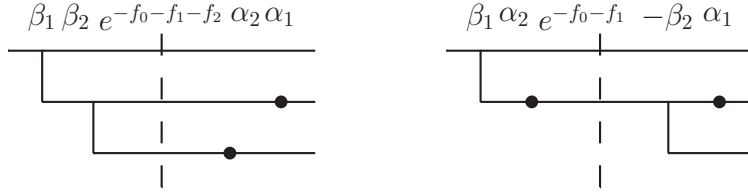
Figure 11: The diagrams for diffractive excitation of both emissions ($|100\rangle \to |111\rangle$) in an ordered three gluon system.

Figure 12: The diagrams for diffractive excitation of one out of two ($|100\rangle \to |110\rangle$) independent emissions.
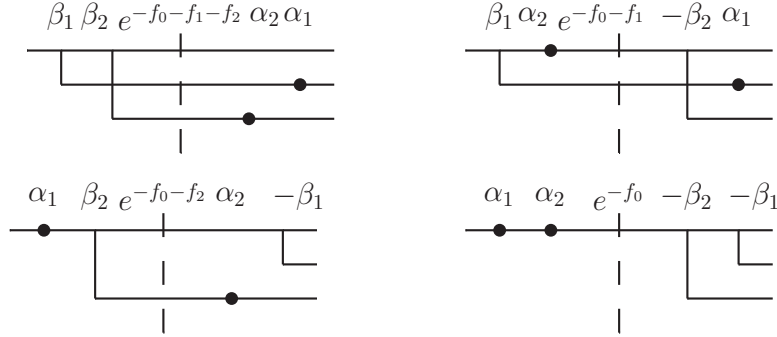
Figure 13: The diagrams for diffractive excitation of two ($|100\rangle \to |111\rangle$) independent emissions.

1. A final state is specified by the *real partons* present in the final state. It will also be important to separate those real emissions, which are the *last gluon* in their chain, from those, called *parent gluons*, which have emitted at least one other real gluon.

   The different diagrams, contributing to the amplitude, may also contain "virtual" gluons, which are emitted but reabsorbed in the cascade. Let $c_{V_i}^2$ denote the probability for emission of a cascade V_i from the real parton i. The virtual cascades can contain more than one emission, and including no emission as representing an empty

cascade, conservation of probability implies that $\sum_{V_i} c_{V_i}^2 = 1$ for each i. The sum is over all possible virtual cascades emitted from the parton i.

2. The contribution from a *last* real parton i is given by

$$\alpha_i \beta_i \sum_{V_i} c_{V_i}^2 (1 - e^{-f_i - F_{V_i}}).$$
(4.18)

3. The contribution from a *parent* real parton i is given by

$$\alpha_i \beta_i \sum_{V_i} c_{V_i}^2 e^{-f_i - F_V}.$$
(4.19)

Comments:

1) All *real* emissions come with a factor $\alpha_i \beta_i$. Either they are emitted before the interaction (weight β_i) and not reabsorbed afterwards (weight α_i), or not emitted before (weight α_i) and then emitted afterwards (weight $-\beta_i$).

2) If *no virtual emissions* were possible, every *last* gluon gives a factor $(1 - e^{-f_i})$. This is the result from interference between contributions from emission before and after the interaction, and can also be interpreted as the amplitude for elastic scattering from the target. Examples are gluon 1 in eq. (4.8) and fig. 7, and gluon 2 in eq. (4.15) and fig. 11.

3) When virtual emissions are possible, the factor $(1 - e^{-f_i})$ for a last gluon is modified. An example is the amplitude $T(|100\rangle \to |110\rangle)$ in eq. (4.13), where gluon 2 can be emitted and reabsorbed by gluon 1, with probability β_2^2. Gluon 2 can only be emitted if gluon 1 is emitted before the interaction, and therefore only affects the last term in the factor $(1 - e^{-f_i})$, changing it to $(1 - e^{-f_1 - f_2})$. Here the suppression factor e^{-f_2} represents the weight for *no* absorption of gluon 2 from the target. (The cross section contains the factor e^{-2f_2}, which is the probability for no absorption.) The probability for not emitting gluon 2 (or for emitting an empty cascade) is $\alpha_2^2 = 1 - \beta_2^2$, and in this case there is no modification of the weight $(1 - e^{-f_1})$. Adding the two contributions can be expressed as the sum in eq. (4.18).

4) The *parent* gluons cannot be emitted after interaction (they would then not be able to emit their daughters), and therefore come with a factor e^{-f_i}, which can be interpreted as the weight for not being absorbed by the target. The effect of a virtual cascade V, is to reduce the weight for no absorption by a factor e^{-F_V}, as expressed in eq. (4.19).

5) These results work also for the original valence particle, if it is treated as a "last" particle for the elastic amplitude, and as a "parent" particle in diffractive excitation, where it has emitted at least one real gluon. (There is no factor $\alpha_0 \beta_0$, as the valence particle is always present.) The difference is only that the two terms in the parenthesis in eq. (4.18) do not correspond to emissions before and after interaction. It is here a contribution from the definition $T = \mathbb{I} - S$, which gives an extra term 1 in the elastic amplitude, reflecting the interference between the incoming and the scattered waves. With this interpretation, an example of the sum over virtual emissions from a parent particle is given by gluon 2 in eq. (4.16) and fig. 12.

4.3 Continuous cascade

We now consider a cascade were every gluon can emit further gluons at every point in the evolution parameter t. This corresponds to an infinite product of evolution operators $U(t)$ with infinitesimal $\beta_i(t)$. In this subsection the gluons are assumed to interact individually, with no effects of screening from neighbouring gluons. Such screening effects are taken into account in the dipole cascade discussed in sec. 4.4. We will here also assume that the cascade only includes gluon emission, and that effects of saturation from gluons joining within the cascades can be neglected.

The infinitesimal values for β_i implies that the corresponding values for α_i are very close to 1, but as there is an infinite set of α_i, the small differences from 1 cannot be neglected. However, as the constraint $\alpha_i^2 + \beta_i^2 = 1$ represents a conservation of probability, and therefore the α:s can be thought of as Sudakov factors, these corrections are automatically taken into account in a MC event generator like DIPSY.

This probabilistic interpretation is also applicable for the emission of virtual cascades V_i, emitted from a real gluon i. Let v denote the individual gluons in the virtual cascade V, and $\bar{v}$ the gluons which *could* have been emitted, either from gluon i or from the gluons in V_i, but were not. In a general situation the probability for the gluon i to emit the cascade V_i is then given by

$$c_{V_i}^2 = \prod_{v \in V_i} \beta_v^2 \prod_{\bar{v} \in \bar{V}_i} \alpha_{\bar{v}}^2. \tag{4.20}$$

Here β_v^2 is the weight for emission and reabsorption of the gluon v in V_i, while $\alpha_{\bar{v}}^2$ is the weight for *no* emission of gluon $\bar{v}$ in $\bar{V}_i$ (where $\bar{V}_i$ is the set of all possible emissions not included in V_i). As in the toy models discussed above, the sum of emission probabilities for all possible cascades from the parent i, adds up to one,

$$\sum_{V_i} c_{V_i}^2 = \sum_{V_i} \left(\prod_{v \in V_i} \beta_v^2 \prod_{\bar{v} \in \bar{V}_i} \alpha_{\bar{v}}^2 \right) = 1, \tag{4.21}$$

as a result of the unitarity relationship between α and β. In the sum over all cascades V we here also include the "empty cascade" V_0, with no emissions, for which $c_{V_0}^2 = \prod_{\bar{v} \in \bar{V}_i} \alpha_{\bar{v}}^2$.

In Appendix A we demonstrate that the rules presented in the previous section also are relevant for a general cascade, and the amplitude for the transition to a real state $|R\rangle$ is given by

$$T_R = \left(\prod_{r \in R} \beta_r \alpha_r \right) \left(\prod_{p \in P} \sum_{V_p} c_{V_p}^2 e^{-f_p - F_{V_p}} \right) \left(\prod_{l \in L} \sum_{V_l} c_{V_l}^2 (1 - e^{-f_l - F_{V_l}}) \right). \tag{4.22}$$

Here R is the set of all "real gluons". V_p is a virtual cascade emitted from a gluon p in the set of "parent gluons", denoted P. l is a gluon in the set L of "last gluons", and V_l is a virtual cascade emitted from l. The sums over V_p and V_l run over all such cascades, including the empty cascades. Finally F_{V_p} and F_{V_l} denote the sum of the relevant terms f_i.

The probalastic interpretation of the factors c_V^2 in eqs. (4.20, 4.21) imply that this result can be generated by a MC event generator. The result can be interpreted as the probability to create the real state, times the probability that none of the parents is absorbed in the interaction with the target, times the probability that the last gluon of each branch in the cascade should interact elastically.

In this section the gluons are assumed to interact individually, with no effects of screening from neighbouring gluons. Such screening effects are taken into account in the dipole cascade discussed in the following section. We have also assumed that the target does not fluctuate like a parton cascade. Two colliding cascades will be discussed in sec. 4.5.

4.4 From gluons to dipoles

4.4.1 Differences from the individual gluon cascade

In the gluon cascade, discussed in the previous section, the interaction of a gluon with the target is not changed by the emission of daughter gluons. The gluons interact individually, with no effects of screening from neighbouring gluons. Such screening effects are taken into account in the dipole cascade, where the screening is determined by the compensating charge in the other end of a dipole. Thus a gluon in a small dipole has a smaller cross section, leading to colour transparency. When a dipole is emitting a gluon, the old dipole disappears, and is replaced by two new dipoles, as discussed in section 3. This is also the case when a virtual cascade is emitted, which implies that some of the real dipoles are no longer present in the interaction with the target. Therefore the interaction amplitude F cannot as easily be separated in one part from the real dipoles and one from the virtual emissions. Some details in the calculations are rather technical and therefore left for appendix A. Here we present first a toy model in sec. 4.4.2, which illustrates the problem, and then a sketch of the full result in sec. 4.4.3.

4.4.2 Toy model with single emission

We consider a simple toy model with two states, an initial single dipole and a state where this is split in two daughter dipoles. Denoting the states by the occupation numbers of the three dipoles, the single dipole state is called $|100\rangle$ and the split state with two new dipoles is called $|011\rangle$. The weight for no absorption is e^{-f_0}, e^{-f_1}, and e^{-f_2} for the three dipoles. The diagrams contributing to diffractive excitation are illustrated in fig. 14. To get a $|011\rangle$ final state, the emission can happen before or after interaction, which gives two contributions to the amplitude. Thus we get

$$T(|100\rangle \to |011\rangle) = -S(|100\rangle \to |011\rangle) = -[\alpha\beta e^{-f_1-f_2} + \alpha(-\beta)e^{-f_0}] = \alpha\beta(e^{-f_0} - e^{-f_1-f_2}) \quad (4.23)$$

We note here that the weight e^{-f_0} cannot be factored out in the same way as in eq. (4.8). It will turn out that the last dipole to split, that is the "second last dipole", will play a similar role also in the general case, discussed in the next section.

Figure 14: The amplitude for the transition $|100\rangle \to |011\rangle$ contains two contributions. The dipole can split by gluon emission before (left) or after (right) the interaction with the target.
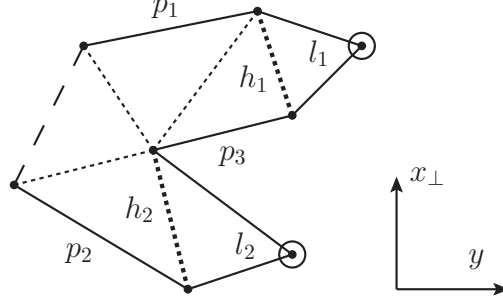
4.4.3 Full dipole cascade

First the notation, illustrated in fig. 15, has to be slightly revised, as the interesting sets of dipoles are different in some aspects. As in the previous section, the set of *real* dipoles in the final state is denoted R. Each branch of a dipole cascade also has a *last* gluon, which can be emitted before or after the interaction, while the rest of the emissions all have to occur before the interaction. In fig. 15 the *last gluons* in the cascade are circled. Each last gluon is connected to two dipoles, formed when the last gluon was emitted. The set of all such dipole *pairs* is denoted L. (Note also that two different last pairs can never have a common dipole.) As in the cascade of independent gluons, the remaining real dipoles will be called *parent* dipoles (included in the set P), although this notation is not fully adequate. They are not parents in the sense that they have split into daughter dipoles. They do, however, connect two gluons, which both have been involved in further emissions.

In the cascade with independent gluons in sec. 4.3, the last emission is the addition of one more gluon, and the previous gluons remain unchanged. As discussed above, in a dipole cascade the last emission will add two new dipoles, and *remove* the emitting dipole. The dipoles which are split in the last emission play a special role, and are called *hidden* dipoles. In diagrams where the last split occurs *before* the interaction, the hidden dipoles do not contribute to the weight for no absorption from the target, but they *do* contribute if the last emission happens *afterwards*. This feature is illustrated in the toy model discussed above.

Virtual cascades in the dipole formalism will also remove the dipole it is emitted from, while adding more dipoles. Therefore the emission of virtual cascades from the "parent dipoles" do not give the factorizing non-interaction weight $\exp(-F_p - F_{V_p})$ obtained in eq. (4.22). Instead we get when the cascade V_p is non-empty, the weight $\exp(-F_{V_p})$, while for the empty cascade we get $\exp(-F_p)$. We therefore here change the notation, and include the empty cascade in the set of all virtual cascades, and define $F_{V_0} \equiv F_p$. This definition implies that the non-interaction weight for the dipole p, including possible virtual emissions, is always given by $\exp(-F_{V_p})$.

We use this notation also when a "last dipole pair" l emits a virtual cascade V_l. Thus, when one or both of the dipoles in the pair l is "emitting" an empty cascade, the non-interaction weight $\exp(-F_{V_l})$ gets a contribution from the still intact dipole(s) in the pair l.

Finally, in case the last dipole pair is produced *after* the interaction, virtual cascades can also be emitted by the hidden dipoles h. As these cascades must be reabsorbed before the last dipole can be emitted, they are restricted to the rapidity range $y > y_l$, where y_l is

Figure 15: A sample dipole cascade with rapidity on the horizontal axis and transverse space on the vertical axis. Full lines are the dipoles left in the final state, while dotted or dashed lines split into new dipoles before the final state. The circled gluons are the ones without children, and are the only gluons which can be emitted both before and after interaction. The emission of a childless gluon creates a pair of dipoles denoted l_i. The childless gluons are emitted by the "hidden" dipoles h_i. The dipoles p_i are the final state dipoles connected only to gluons with children. Dipoles that always split before interaction are marked with thin dotted lines, and the long dashed line is the original dipole.

the rapidity of the last gluon. Also here the non-interaction weight $\exp(-F_{V_h})$ is defined to equal $\exp(-F_h)$, when the cascade V_h is the empty cascade. With this notation the result in eq. (4.22), is for a dipole cascade replaced by the following expression:

$$T_R = \left(\prod_{r\in R} \beta_r \alpha_r\right) \left(\prod_{p\in P}\sum_{V_p} c_{V_p}^2 e^{-F_{V_p}}\right) \left(\prod_{l\in L}\sum_{V_l} c_{V_l}^2 \sum_{V_h(y>y_l)} c_{V_h}^2 \left(e^{-F_{V_h}} - e^{-F_{V_l}}\right)\right). \quad (4.24)$$

Note here that there is no product over hidden dipoles, as the hidden dipole h is specified by the last pair l. The last factor, $(e^{-F_{V_h}} - e^{-F_{V_l}})$, is a generalization of the result in the simple toy model. The details of the calculations are presented in appendix A.

Note that, like for the independent gluon cascade in eq. (4.22), in the derivation of these results it is assumed that the virtual cascade from one emission is independent of the virtual cascade from another emission. Thus the result corresponds to a cascade without saturation effects from gluons which can join, or dipoles which swing. These effects are further discussed in secs. 5 and 7.2.

4.5 Target cascade

Up to now the target has been described as a potential without internal structure. It can however also be described by a superposition of virtual cascades, V_t, in the same way as the projectile. For single diffractive excitation, where the target is scattered elastically, the sum over virtual cascades from the target particle should be summed over at amplitude level (*cf* eq. (2.6)). The amplitude can thus be written as an average over target configurations V_t, with weights $c_{V_t}^2$, where all interaction amplitudes F now depend on the target cascade.
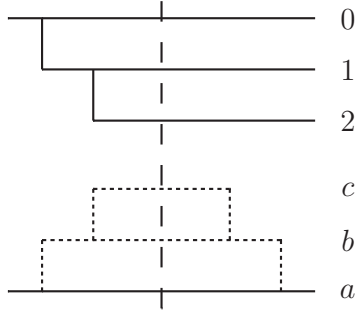
Figure 16: A diagram contributing to single diffractive excitation in a collision between two cascades, where the target is scattered elastically. Labeling the partons in the upper projectile state 0, 1, and 2, and labeling the partons in the target cascade a, b, and c, with a the incoming parton, the amplitude corresponding to this diagram is $\beta_1\beta_2\beta_b\beta_c\exp(-F)\alpha_1\alpha_2\beta_b\beta_c$, with $F = f_{0a} + f_{1a} + f_{2a} + f_{0b} + f_{1b} + f_{2b} + f_{0c} + f_{1c} + f_{2c}$.

For a dipole cascade we then get the amplitude

$$T_R = \sum_{V_t} c_{V_t}^2 \left(\prod_{r\in R} \beta_r\alpha_r \right) \left(\prod_{p\in P} \sum_{V_p} c_{V_P}^2 e^{-F_{V_p,V_t}} \right) \left(\prod_{l\in L} \sum_{V_l} c_{V_l}^2 \sum_{V_h(y>y_l)} c_{V_h}^2 \left(e^{-F_{V_h,V_t}} - e^{-F_{V_l,V_t}}\right) \right).$$
(4.25)

$F_{X,T}$ is here the interaction amplitude between the virtual projectile cascade X and the target virtual cascade T, given as a sum $F_{X,T} = \sum_{i,j} f_{i,j}$ over dipoles i in X and j in T.

5. Implementation in DIPSY

The amplitude in eqs. (4.24, 4.25) can be used to generate diffractive events with the DIPSY event generator [47]. The approach will be to first select a real cascade with the weight $\prod_{r\in R} \beta_r^2\alpha_r^2$, as it will appear in the squared amplitude, and then perform the sum over virtual cascades to determine the amplitude for this real state.

Real Cascade. First note that in a continuous cascade, each β is small, and each individual α is very close to 1. So the weight for the real cascades is essentially $\prod_{r\in R} \beta_r^2$. This weight does not include the probability that no further cascade is emitted after R. To get the correct weight, any time the Monte Carlo generates a certain cascade R it should count towards the probability for that final state, no matter if the cascade goes on to generate more gluons afterwards. This is done by first generating a cascade D with DIPSY as normal up to a maximum rapidity $y_{\max}$, and return a random sub-cascade $R \subset D$, weighted by the total number of sub-cascades of D.

As discussed in sec. 3.3, the structure of inelastic final states is determined by the "backbone" or "$k_\perp$-changing" emissions. Presuming that diffraction is the shadow of absorption to inelastic states, we here conjecture that also diffractive states are specified by their $k_\perp$-changing backbone gluons. Therefore real sub-cascades which contain softer,

not $k_\perp$-changing, emissions have to go through the same reweighting procedure as the non-diffractive final states, as discussed in sec. 3.3 and fully described in ref. [47].

The sum over virtual cascades. For single diffractive excitation the sums over virtual cascades from the final excited state R all come with weights c^2, and can be calculated directly from DIPSY. The sum over target cascades $\sum_{V_t}$ is independent of the excited state, and these cascades can be pre-generated and reused for each real state to save cpu-time.

For each real state, the subsets P and L are identified, and virtual cascades V_p, V_l, and V_h are generated. Each of the pre-generated target cascades V_t is paired up with a virtual cascade, and the factors $e^{-F_{V_p,V_t}}$ and $(e^{-F_{V_h,V_t}} - e^{-F_{V_l,V_t}})$ in the amplitude in eq. (4.25) are calculated and multiplied together. The average over all the virtual cascades is then squared, and added to the weight for the real cascade $(\prod_r \beta_r^2)$ discussed above, to give the total weight for the real state.

Saturation effects. In the Lund cascade model saturation effects are included within the cascade evolution via the dipole "swing" (see sec. 3.2), in addition to the effect from multiple subcollisions. The result in eq. (4.25) is valid for a linear cascade. In the MC implementation, swings are included in each virtual cascade from each subset P, h, l, but swings between these virtual cascades are not considered in the current implementation. Swings are also included in the virtual cascade V_t from the target.

In DIS, this omission is expected to be of negligible importance. First each real chain end l gives a small factor $(1 - e^{F_{V_l,V_t}})^2$, and therefore events with two or more chain ends (corresponding to multiple pomeron exchange) are suppressed, unless Q^2 is very small. Further, a large contribution to the cross section comes from real states with 0 or 1 emission from the $q\bar{q}$ pair, and in those cases there are no parent emissions P, and there can be no swing between different subsets of the real cascade. For states with two or more gluons, there are corrections for the swing, but the $1/N_c^2$ suppression makes it small as long as the emissions are not too many. To further minimize the correction, the maximum rapidity for the generated projectile cascades, $y_{\max}$, is chosen as close to the real state as possible, to give the virtual cascades from the real state little room to give saturation effects. This is compensated by a longer evolution of the elastically scattered target proton, which includes the swing.

In the case of a diffractively excited proton, saturation is a larger effect as the gluon density is higher and because the average dipole size is larger. Its effect is, however, reduced because diffractive excitation is dominated by peripheral collisions with relatively few interacting dipoles. For central collisions with large interaction probability, diffractive scattering is dominantly purely elastic. A method to calculate the amplitude taking full account of saturation is introduced in section 7.2, but this is not implemented in the present MC.

FSR and hadronisation As in the application of the DIPSY MC for generation of non-diffractive final states [47], final state radiation is included in the same way as for the Linked Dipole Chain model [64, 65] in ARIADNE [66], and finally hadronisation using the Lund string model [67, 68] implemented in PYTHIA8 [45, 69].

With these steps it is possible to generate full exclusive single diffractive final states from the DIPSY event generator. We want to stress that *no new parameters* are introduced, which can be tuned to experimental data. All parameters were previously determined by total and elastic cross section as functions of $\sqrt{s}$, and to some extent by exclusive non-diffractive data and elastic reactions. Final state radiation in ARIADNE and hadronization in PYTHIA have been tuned to exclusive LEP data.

6. Early results

As emphasized above, the cross sections for diffractive excitation are in our formalism, via the optical theorem, fully determined by the projectile and target cascades, and their absorption into non-diffractive inelastic reactions. For DIPSY, the inelastic absorption is tuned to inclusive observables and pp minimum bias multiplicity in [47], and thus no additional parameters are introduced in the extension to diffractive final states. It should also be noted that tuning to experiments was done with respect to pp data only, the only exception being the total $\gamma^* p$ cross section (or equivalently F_2) as function of Q^2.

In this section we show some early results with low statistics as proof of concept. We will continue with improvements in the present version of the MC implementation, which will facilitate predictions for higher collision energies and excitation masses.
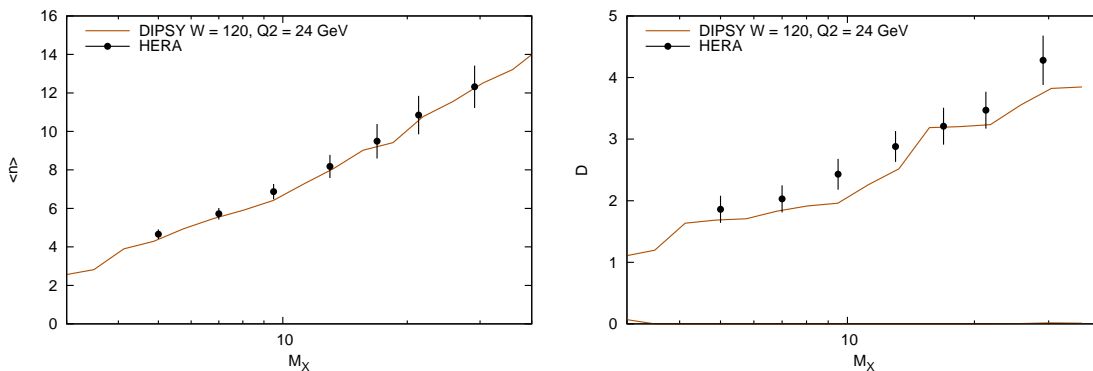
6.1 DIS

Experimental results for diffractive excitation of the photon in DIS are available from HERA. Unfortunately a diffractively excited proton is mainly outside the acceptance of the HERA detectors. Results for inclusive diffractive cross sections and for $d\sigma_{SD}/dM_X^2$ could be easily obtained from the original DIPSY MC, and were presented in ref. [21], in good agreement with data from HERA. In the new formalism it is also possible to obtain information about the partonic content of the diffractive states. In fig. 17 we show our result for the distribution in $\ln M_X^2$ at $W = 120$ GeV and $Q^2 = 24\,\text{GeV}^2$. The figure also shows the separate contributions from states with 0, 1 and ≥ 2 gluons besides the $q\bar{q}$ pair initially coupled to the virtual photon. We see that there is a bump at $M_X^2 \approx Q^2$, which corresponds to final states formed by the initial $q\bar{q}$ state. This bump is followed by a more flat distribution, obtained from states including also one or more gluons. As expected, states with more gluons become increasingly important for higher masses M_X. The distribution in the figure has a smooth cut off around 50 GeV, due to the Lorentz frame used in the simulation, which limits the rapidity range for the gluons in the excited state.

Some results for the properties of the hadronic final state, obtained after final state radiation and hadronization, are presented in figs. 18 and 19, and compared with HERA data from H1 [70, 71]. In all cases the results are obtained for $W = 120$ GeV and $Q^2 = 24\,\text{GeV}^2$. In fig. 18 we show the average total charged multiplicity and its fluctuations, as function of excited photon mass M_X in single diffractive excitation. We see here a very good agreement between our results and the experimental data, both for the average and for the fluctuations. Fig. 19 shows the average charged multiplicity as function of rapidity,
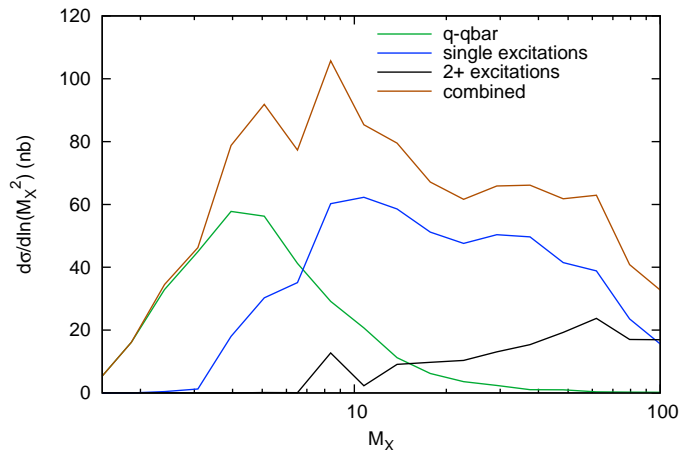
Figure 17: The distribution in $\ln M_X^2$ for single diffractive excitation in DIS at $W = 120$ GeV and $Q^2 = 24\,\mathrm{GeV}^2$. Besides the total result, also the contributions from $q\bar{q}$ states with no gluon emission, 1 gluon emission, and 2 or more gluon emissions are indicated. The distribution has a smooth cut off above 50 GeV due to the Lorentz frame used is the simulation.
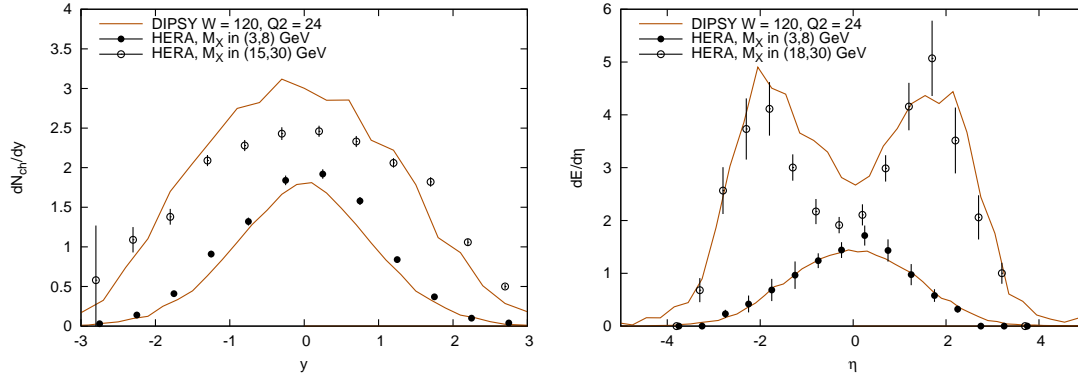

Figure 18: The average total charged multiplicity (left) and its fluctuations (right) as function of excited photon mass M_X in single diffractive DIS at HERA [70].

and average energy flow as function of pseudorapidity, in two bins of M_X. Also here we find a rather good agreement with data. The fact that it agrees for both the multiplicity and the energy flow, indicates that also the average transverse momentum has to be correctly reproduced.

6.2 pp and $p\bar{p}$ collisions

Also in colliders for pp or $p\bar{p}$ collisions most detectors have limited acceptance for a diffractively excited proton. At the CERN $p\bar{p}$ collider, results for distributions in pseudorapidity were presented from the UA5 and UA4 detectors [3,4]. Fig. 20 shows η-distributions for single diffraction in two mass bins with $\langle M_X \rangle = 100$ GeV and $\langle M_X \rangle = 140$, in $p\bar{p}$ collisions at $W = 546$ GeV. We see that a rapidity plateau with $dN_{ch}/d\eta \sim 2.5$ is developed for
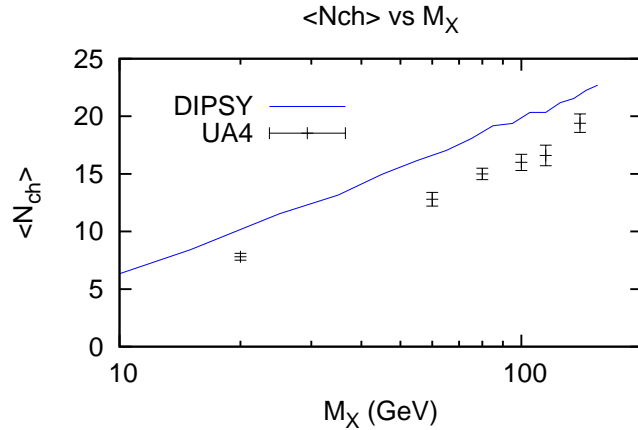
Figure 19: The average charged multiplicity as function of rapidity in bins of M_X (left) [70], and average energy flow as function of pseudorapidity in bins of M_X (right) [71]. The results correspond to $W = 120$ GeV and $Q^2 = 24$ GeV^2.
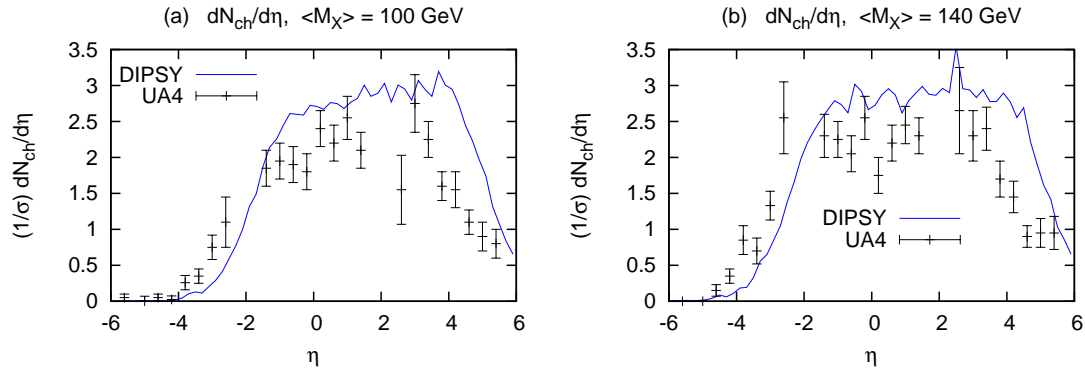
Figure 20: Pseudorapidity density $dN_{ch}/d\eta$ (in the total cms) in single diffraction in two mass bins with $\langle M_X \rangle = 100$ GeV and $\langle M_X \rangle = 140$, in $p\bar{p}$ collisions at $W = 546$ GeV. The results from DIPSY are compared with data from UA4 [3]. The excess of particles at large η is related to the lack of a leading baryon in our model, see the main text.

larger M_X-values, in fair agreement with the experiment. We also note that the simulation gives a surplus of particles at high η, amounting to approximately one extra particle. This fact is related to the lack of a leading baryon in our model. This baryon is expected to take a significant fraction of the forward energy, and thus reduce the particle density for large η-values. The lacking baryon is a consequence of our simple proton wavefunction, which contains only gluons. This was motivated by the fact that after a long cascade evolution, the resulting parton distribution at small x is rather insensitive to the initial wavefunction. The particles at high η in fig. 20 do, however, depend sensitively on the large x partons.

The lack of quarks can also explain our general overestimate of the charged multiplicity, which is almost constant over a wide range of M_X, as can be seen in fig. 21. Our diffractive final states will always contain a double string connecting a leading gluon in the backward direction with the remnant, while in reality there will also be diffractive states with a

Figure 21: The average charged multiplicity as a function of M_X generated by DIPSY and compared to data from UA4 [3].

leading quark, giving rise to only one string and, therefore, approximately only half the multiplicity. The fraction of such states should decrease with increasing M_X and the rise of the multiplicity is mainly determined by gluonic components, but it may very well explain the constant surplus multiplicity in our model. In addition, the fact that a leading quark has a harder fragmentation function may partly explain why our simulations undershoots data at large negative rapidities in fig. 20.

The lack of quarks has also effects in other places, where large x-values are important, *e.g.* for jets with very high $p_\perp$, and in future improvements we will have to include quarks in the proton wavefunction.

7. Future developments

We here discuss some effects and reactions, which are not implemented in the present MC, but which can be included in future versions.

7.1 Double diffraction

The results for single diffractive excitation, discussed in the previous sections, can also be generalized to double diffraction. The result is, however, numerically more complicated and the implementation in a MC would be more time consuming. For simplicity we here discuss the result for independent gluon cascades, but the result can be directly generalized to dipole cascades. Consider a diffractive reaction in which the projectile is excited to a real cascade R_p, and the target to a real cascade R_t. The number of "last" gluons is n_p and n_t respectively. The last gluons can be emitted either before or after the interaction, which implies that there are $2^{n_p+n_t}$ different diagrams contributing to the amplitude. For a specific diagram the sets of last gluons emitted *before* the interaction in the projectile and target cascades are denoted B_p and B_t. Each pair of two last gluons in these sets, b_p from the

projectile and b_t from the target, contributes a weight $\sum_{V_{b_p}} c_{V_{b_p}}^2 \sum_{V_{b_t}} c_{V_{b_t}}^2 \exp(-F_{V_{b_p},V_{b_t}})$. Here the sums run over all virtual cascades emitted from b_p and b_t. (We here use the notation introduced in sec. 4.4.3, and let $F_{V_{b_p},V_{b_t}}$ include contributions from the parent gluons b_p and b_t.) In addition these gluons also interact with all "parent" gluons coming from the other side. The "last" gluons, which are emitted after the interaction, do not take part in the interaction, and give only the factor $(-1)^N$, where N is the number of such gluons in the diagram.

The parent gluons also interact with each other in the same way as for single diffraction. In obvious notation the total contribution from this diagram is

$$
(-1)^N \left(\prod_{r_p \in R_p} \beta_{r_p} \alpha_{r_p} \right) \left(\prod_{r_t \in R_t} \beta_{r_t} \alpha_{r_t} \right)
$$
$$
\times \prod_{p_p \in P_p} \sum_{V_{p_p}} c_{V_{p_p}}^2 \prod_{p_t \in P_t} \sum_{V_{p_t}} c_{V_{p_t}}^2 \prod_{b_p \in B_p} \sum_{V_{b_p}} c_{V_{b_p}}^2 \prod_{b_t \in B_t} \sum_{V_{b_t}} c_{V_{b_t}}^2
$$
$$
\times e^{(-F_{V_{p_p},V_{p_t}} - F_{V_{p_p},V_{b_t}} - F_{V_{b_p},V_{p_t}} - F_{V_{b_p},V_{b_t}})} \tag{7.1}
$$

Summing over the $2^{n_p+n_t}$ different diagrams then gives the total amplitude for the double diffraction final state R. The result does not simplify to a factorized expression as the result for single diffraction in eq. (4.22), but it can still be calculated in a MC, only more time consuming.

7.2 Full account of saturation effects

In sec. 4 the cascade evolution was assumed to be linear, that is, each gluon will radiate (or each dipole split) independently from the rest of the cascade. This is a good approximation for γ^*p, with an excited photon with moderate or high Q^2, but in the case of pp scattering, non-linear effects play a very important role in diffractive scattering [22]. Diffractive excitation is very much suppressed in central collisions, where diffraction is dominated by elastic scattering. Thus diffractive excitation is largest in peripheral collisions, where saturation is not equally important. In the present MC, saturation effects are, besides from multiple subcollisions in the Lorentz frame used, also included with swings within individual sub-cascades, as described in sec. 5. We expect this to account for most of the saturation effects in events with not too high masses M_X. However, for excitation to higher masses swings between dipoles in *different* cascades may also be important, and we here discuss how it is possible to include these interactions, and thus take full account of saturation effects.

This problem is similar to the problem with double diffraction discussed above, in that the sum of contributions from all possible diagrams does not factorize. Consider a real cascade with $n \geq 2$ branches ending in childless gluons l_i. As described in sec. 4, these gluons can be emitted either before or after the interaction. This implies that there are 2^n different diagrams which contribute to the amplitude. Virtual sub-cascades can be emitted from a childless gluon if this is emitted before interaction, but not if it is emitted after the interaction. If the sub-cascades do not interact with each other, the result factorizes as shown in eq. (4.22) or (4.24). This is no longer the case if the evolution

of one virtual sub-cascade depends on whether another childless gluon is emitted before or after the interaction with the target. This implies that all the 2^n different diagrams must be calculated separately, and added to give the full production amplitude. This is not a problem in principle, but it becomes numerically difficult as the virtual cascades have to be calculated for each of the 2^n possible combinations of childless gluons emitted before the interaction. It becomes very time consuming, unless an efficient weighting system is introduced, which favours the generation of states with a relatively high production probability.

7.3 Quarks in the proton wavefunction

The model for a proton wavefunction in the MC contains only gluons. The motivation is that gluons dominate the cascades at high energy, and for evolutions down to small x, the result is rather insensitive to the exact starting configuration. For diffractive events this motivation is only relevant for excitation to large masses. For lower M_X, experimental results are consistent with particle production from a single string, stretched between a pulled out quark and the proton remnant [30]. To describe these states it is necessary to include quarks in the initial proton wavefunction. This problem will be addressed in future work.

7.4 Formalism combining diffractive and non-diffractive events

We have in this paper discussed diffractive events with one or more pomerons exchanged. The pomerons are ladders formed by gluon pairs, which mediate momentum exchange and thus are able to excite the projectile to higher mass. In our earlier treatment of non-diffractive reactions [47], we have studied events where one or more dipole branches interact with the target via gluon exchange. This exchange causes a colour connection between the projectile cascade and the target, and provides momentum which puts the interacting dipole branch on shell. Branches which do not interact in this way are treated as virtual, and reabsorbed in the projectile state.

We here discuss how it is possible to include exchange of both (uncut) pomerons and gluons in a unified formalism. An example of an event with both types of exchange in a single event, is shown in fig. 22. There is no gap in the event, but the branch connected to the pomeron is coming on shell, increasing the multiplicity. In the formalism in ref. [47] the probability for this final state is included in the non-diffractive cross section, but the branch interacting with the pomeron is treated as virtual, and neglected in the final state. Although not modifying the inclusive non-diffractive cross section, this implies a small underestimate of the multiplicity in these events. It would, however, not affect any results presented in this paper. A further discussion about this combined formalism, and how it could be implemented in the event generator, is presented in appendix B.

7.5 Hard diffraction and multiple gap events

The present version of the DIPSY MC generates unbiased events. This implies that it is quite inefficient for producing hard diffraction, like events with high $p_\perp$ jets, for which some kind of theoretical trigger would be needed. It also does not include multiple gap events.
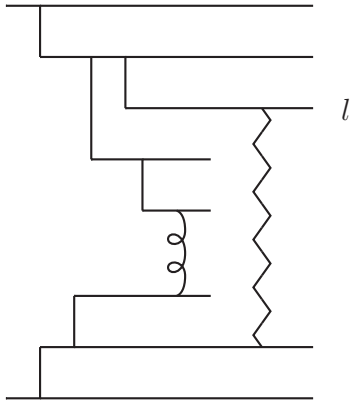
Figure 22: A cascade with both colourful and colour neutral exchange with the target. The spiral line represents exchange of a single gluon with the target, which gives a colour connection. The zigzag line represents exchange of a colour neutral pomeron. It transfers momentum implying that the branch ending in the gluon marked l, can come on shell, but it does not result in a colour connection between this gluon and the target.

Here we believe that the formalism described in sec. 7.4, can be generalized to describe events with several uncut pomerons, including diffractive events with more than one gap, or double diffraction with overlapping diffractive systems.

8. Conclusions

In this paper we describe a formalism, in which exclusive final states in diffractive excitation can be determined from basic QCD dynamics, BFKL evolution and saturation. Although diffraction is basically a quantum-mechanical phenomenon with strong interference effects, we show here how it is still possible to calculate the different interfering components to the amplitude in a MC simulation, add them with proper signs, and thus calculate the reaction cross section for exclusive diffractive final states.

Our formalism is based on the Good–Walker formalism for diffractive excitation, and it is assumed that the virtual parton cascades represent the diffractive eigenstates defined by a definite absorption amplitude, in analogy with refs. [18,20–22]. Thus we here assume that events with large rapidity gaps can be understood as analogous to diffraction in optics, with matrix elements determined by absorption into inelastic channels via the optical theorem. This is also the case for the Regge formalism, where the calculation of diffractive cross sections is based on the AGK cutting rules and Mueller's triple-Regge formalism. In ref. [23] we also conjecture that the Good–Walker and triple-pomeron formalisms actually are different views of the same dynamical phenomenon.

Also a description where gaps are the result of "soft colour reconnection" in initially colour connected inelastic events, has successfully described many experimental observations [24, 25]. This is also the case for a description of gap events in terms of projectile-pomeron collisions [41], which is implemented in a number of event generators. The true

nature of rapidity gap events is therefore still not fully revealed. An essential feature of our scheme is here that the result is fully determined by the inelastic reactions, with no extra tunable parameters, pomeron flux factors or pomeron parton distributions, which have to be tuned to data.

The formalism is based on the Lund dipole cascade model, which in turn is based on BFKL evolution and saturation, and is implemented in the DIPSY event generator [46,47]. The model is a generalization of Mueller's dipole cascade model [49–51], including also non-leading effects and saturation effects within the evolution. It has previously been successfully applied to inclusive diffractive cross sections in DIS and pp collisions [21,22], and later also to exclusive final states in non-diffractive events [47]. The assumption that the interaction is dominated by absorption into inelastic channels implies that all contributions to the amplitudes are real, and therefore can be added with their relative signs, and afterwards squared to give the relevant reaction cross sections. This feature also implies that it is possible to calculate the Fourier transform of the b-distribution, and determine the t-dependence (some results are presented in ref. [22]).

We here note that, as discussed in refs. [60,61], the structure of non-diffractive final states is determined by the "backbone" or "$k_\perp$-changing" emissions. For exclusive final states, final state radiation has to be added with Sudakov form factors, thus not changing the inclusive cross sections. Assuming that diffraction is the shadow of absorption to inelastic states, we here implicitly assume that also diffractive states are specified by their $k_\perp$-changing backbone gluons, where final state radiation and hadronization must be added to get the detailed final states.

We show in this paper some early results for single diffraction in DIS and pp collisions, with comparisons to experimental data. As emphasized above, these results were obtained without introducing any new parameters to the model, and the predictions for exclusive diffractive observables are entirely determined by tuning to non-diffractive and elastic data.

In the near future we plan to present more detailed analyses of the model, include quarks in the proton wavefunction, and make predictions for LHC energies. We also want to compare our results with those from other approaches, *e.g.* PYTHIA [45] and SHRIMPS [16]. In the somewhat longer perspective we may include double diffraction, multiple gap events, and a formalism combining diffractive and non-diffractive events, as described in sec. 7. This development will need a significant improvement of the algorithms. Hard diffraction would in addition need some kind of theoretical trigger.
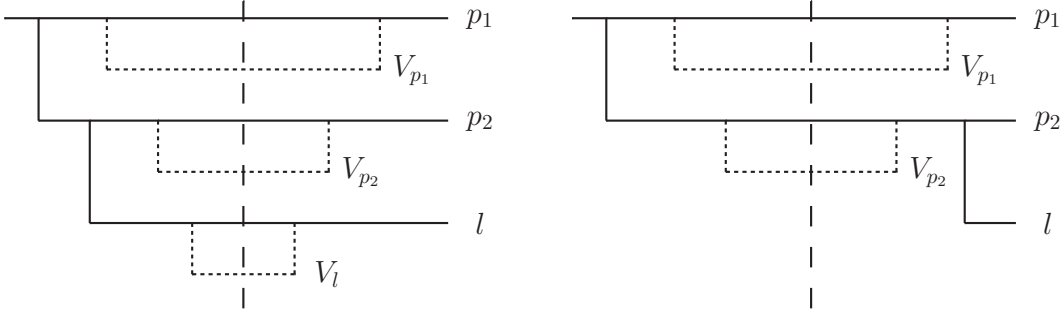
Acknowlegments

Appendices

A. Final states for a full continuous cascade

We here derive the results for the transition amplitudes in eqs. (4.22,4.24). For simplicity

Figure 23: The final state $R = P \cup l$ gets contributions from diagrams where l is emitted before interaction (left) and after interaction (right). Due to ordering, virtual cascades from l (such as V_l) are only possible when l is emitted before interaction.

we only discuss the independent gluon cascade. The modifications in a dipole cascade were discussed in sec. 4.4.3.

We first study the simpler case with a single real chain, where the set of "last" gluons, L, contains only a single gluon l. This is the case illustrated in fig. 23. The emission structure of the real gluons R can then only be in two configurations: either they are all emitted before interaction (left diagram of fig. 23), or the last gluon, l, is emitted afterwards (right diagram of fig. 23). As discussed above, the "parent" gluons must always be emitted before interaction, to give the last gluon a chance to be emitted.

We begin with the diagram on the left of fig. 23, where the last real gluon is emitted *before the interaction*. This part of the S-matrix must include a sum over all possible virtual cascades V_i, emitted from the partons, i, in the real cascade. The emission probability for a particular virtual cascade V_i is given by $c_{V_i}^2$ defined in eq. (4.20), which satisfy the constraint $\sum c_{V_i}^2 = 1$ where the sum runs over all virtual cascades for a fixed real parton i. The contribution to the S-matrix from all diagrams of this type is given by

$$
\begin{aligned}
S_B &= \prod_{r \in R} \left(\beta_r \alpha_r \sum_{V_r} c_{V_r}^2 e^{-(f_r + F_{V_r})} \right) \\
&= \left(\prod_{r \in R} \beta_r \alpha_r \right) \left(\prod_{p \in P} \sum_{V_p} c_{V_p}^2 e^{-f_p - F_{V_p}} \right) \left(\sum_{V_l} c_{V_l}^2 e^{-f_l - F_{V_l}} \right).
\end{aligned} \tag{A.1}
$$

Here f_r and $F_{V_r} = \sum f_v$ denote the Born-level interactions, with the sum running over all gluons in the cascade V_r. Thus the factor $e^{-(f_r + F_{V_r})}$ represents the weight for no inelastic interaction by the gluon r, or by its associated virtual cascade V_r. The sums in eq. (A.1) run over all possible virtual cascades, with their respective probabilities. In the last line we have separated the product over real gluons into a product over parent gluons times a contribution from the last gluon l. We have also pulled out the product over $\beta_r \alpha_r$.

The second contribution to the S-matrix, where l is emitted *after the interaction* (see right diagram of fig. 23), contains an extra (-1), and allows only virtual cascades from the

"parent" gluons p. Thus this contribution is

$$S_A = (-1) \left(\prod_{r \in R} \beta_r \alpha_r \right) \left(\prod_{p \in P} \sum_{V_p} c^2_{V_p} e^{-f_p - F_{V_p}} \right). \tag{A.2}$$

Adding the contributions in eqs. (A.1, A.2) gives the S-matrix element for transition from an incoming state $|0\rangle$ to an excited state $|R\rangle$. For a non-elastic transition we have $T = -S$, which gives the result

$$T(|0\rangle \to |R\rangle) = -(S_B + S_A) = \left(\prod_{r \in R} \beta_r \alpha_r \right) \left(\prod_{p \in P} \sum_{V_p} c^2_{V_p} e^{-f_p - F_{V_p}} \right) \left(1 - \sum_{V_l} c^2_{V_l} e^{-f_l - F_{V_l}} \right)$$

$$= \left(\prod_{r \in R} \beta_r \alpha_r \right) \left(\prod_{p \in P} \sum_{V_p} c^2_{V_p} e^{-f_p - F_{V_p}} \right) \left(\sum_{V_l} c^2_{V_l} (1 - e^{-f_l - F_{V_l}}) \right). \tag{A.3}$$

In the last equality we have here used the relation $\sum c^2_{V_l} = 1$.

In a general real cascade there may be several branches, which end in a "last" gluon. As before, the parent gluons in the real cascade, which are not the last ones in their branch, have to be emitted before the interaction. Otherwise their children could not be emitted. As in the simpler example above, they must all contribute a factor $(\sum_{V_p} c^2_{V_p} e^{-f_p - F_{V_p}})$. The last gluons can all be emitted either before or after the interaction, and they will therefore all give a factor $(-\sum_{V_l} c^2_{V_l} (1 - e^{-f_l - F_{V_l}}))$ to the S-matrix element. As the sign of the transition amplitude is not important for the reaction rate, we get for a cascade of independent gluons the final result (*cf* eq. (4.22))

$$|T(|0\rangle \to |R\rangle)| = \left(\prod_{r \in R} \beta_r \alpha_r \right) \left(\prod_{p \in P} \sum_{V_p} c^2_{V_p} e^{-f_p - F_{V_p}} \right) \left(\prod_{l \in L} \sum_{V_l} c^2_{V_l} (1 - e^{-f_l - F_{V_l}}) \right) \tag{A.4}$$

B. Events with both diffractive and non-diffractive subcollisions

In the Good-Walker formalism only diffractive states are considered. Cascades which get colour-connected to the target are treated as absorbed, and removed from the incoming wave. The coherent sum of cascades forming the proton wavefunction is distorted when different components are absorbed with different probabilities. This distortion, which leads to diffractive excitation, is described by a non-unitary S-matrix, which is insensitive to the nature of the absorbed states.

Within the Lund dipole cascade formalism it is also possible to describe the exclusive non-diffractive states responsible for the absorption [47], and it is possible to combine the two descriptions in a unified formalism, which can be implemented in the event generator DIPSY. In such a scheme the interaction will be described by a unitary S-matrix.

Toy model   To illustrate the method we first study the simple toy model discussed in sec. 4.2.1. In this model there is an initial valence particle, which is able to emit a gluon. There are two different diffractive states, $|1, 0\rangle$ and $|1, 1\rangle$, where the numbers 0 and 1 denote

an empty or occupied parton state. We now extend the set of states, and let the number 2 indicate a parton which has interacted via gluon exchange, and is attached to the target. Thus we have 6 different states:

$$|1,0\rangle, \quad |1,1\rangle, \quad |1,2\rangle, \quad |2,0\rangle, \quad |2,1\rangle, \quad |2,2\rangle. \tag{B.1}$$

We have also to generalize the evolution operator $U(-\delta, -\infty)$ in eq. (4.3), which describes the emission of a gluon. The valence particle can emit a gluon with weight β, if the gluon state is empty. This is possible also if the valence parton is attached to the target, and we therefore have

$$U(-\delta, -\infty)|1,0\rangle = \alpha|1,0\rangle + \beta|1,1\rangle, \quad U(-\delta, -\infty)|2,0\rangle = \alpha|2,0\rangle + \beta|2,1\rangle. \tag{B.2}$$

All other states already contain an emitted gluon, and are unaffected by $U(-\delta, -\infty)$.

The interaction with the target described by U_{int} has now, besides the elastic non-interaction weights e^{-f_0} and e^{-f_1} in eq. (4.4), also non-diffractive interactions transforming a free valence parton to an attached one, with weight $\sqrt{1 - e^{-2f_0}}$, and similarly transforming a free gluon to an attached gluon with weight $\sqrt{1 - e^{-2f_1}}$. This implies that U_{int} can be written in a factorized form $U(-\delta, +\delta) = U_{\text{int}} = U_{\text{int},0}U_{\text{int},1}$, where

$$U_{\text{int},0}|1,i\rangle = \gamma_0|1,i\rangle + \delta_0|2,i\rangle, \qquad U_{\text{int},1}|j,1\rangle = \gamma_1|j,1\rangle + \delta_1|j,2\rangle. \tag{B.3}$$

Here $\gamma_i = e^{-f_i}$ is the non-absorption amplitude, and $\delta_i = \sqrt{1 - e^{-2f_i}}$ the non-diffractive interaction amplitude. $U_{\text{int},0}$ does not act on gluon 1 and vice versa. Note that

$$\gamma_i^2 + \delta_i^2 = 1,$$

as now U_{int} is a unitary operator.

Finally the evolution after the interaction is given by $U(+\infty, +\delta) = U^\dagger(-\delta, -\infty)$, which implies that the non-diagonal elements have changed sign. (We have defined the phases such that α and β are real.) Note that since $U(-\delta, -\infty)$ can only emit free gluons, an attached gluon cannot be absorbed by $U(+\infty, +\delta)$. The unitary S-matrix is given by $S = U^\dagger(-\delta, -\infty)U_{\text{int}}U(-\delta, -\infty)$, and it is straightforward to read off the transition amplitudes for an incoming state with a single valence parton:

$$S(|1,0\rangle \to |1,0\rangle) = \gamma_0(\alpha^2 + \beta^2\gamma_1) = e^{-f_0}\left(\alpha^2 + \beta^2 e^{-f_1}\right)$$

$$S(|1,0\rangle \to |1,1\rangle) = -\alpha\beta\gamma_0(1 - \gamma_1) = -\alpha\beta e^{-f_0}\left(1 - e^{-f_1}\right)$$

$$S(|1,0\rangle \to |1,2\rangle) = \beta\gamma_0\delta_1 = \beta e^{-f_0}\sqrt{1 - e^{-2f_1}}$$

$$S(|1,0\rangle \to |2,0\rangle) = \delta_0(\alpha^2 + \beta^2\gamma_1) = \sqrt{1 - e^{-2f_0}}\left(\alpha^2 + \beta^2 e^{-f_1}\right)$$

$$S(|1,0\rangle \to |2,1\rangle) = -\alpha\beta\delta_0(1 - \gamma_1) = -\alpha\beta\sqrt{1 - e^{-2f_0}}\left(1 - e^{-f_1}\right)$$

$$S(|1,0\rangle \to |2,2\rangle) = \beta\delta_0\delta_1 = \beta\sqrt{1 - e^{-2f_0}}\sqrt{1 - e^{-2f_1}}$$

We note here that the amplitudes for elastic scattering and diffractive excitation, in the first two lines, agree with the result in sec. 4.2.1. The inclusive non-diffractive cross section also agrees with the eikonal result $d\sigma_{\text{inel}}/d^2b = \langle 1 - e^{-2F} \rangle = \alpha^2(1 - e^{-2f_0}) + \beta^2(1 - e^{-2f_0 - 2f_1})$, used in earlier publications. However, in our analysis of exclusive non-diffractive final states in ref. [47], the possibility for momentum exchange which can put a virtual branch on shell, as the emitted gluon in state $|2,1\rangle$, was not included. Thus in the present version of the DIPSY event generator the cross section for the state $|2,0\rangle$, with only the valence parton connected to the target, is overestimated and given a probability representing both states $|2,1\rangle$ and $|2,0\rangle$.

General cascade   The above result generalises easily to a full cascade of multiple chains with continuous emissions. For clarity we here show the result for cascades of independent gluons, as discussed in sec. 4.3. We let N denote the non-diffractive cascade, consisting of the interacting gluons (set I) and their ancestors (set A). As before R is the set of gluons in the branches which come on shell via pomeron exchange, with L denoting the last gluons in its branch and P denoting their parents (including grandparents etc., but not including any gluon in N). The generalization of eq. (4.22) then reads

$$S(|0\rangle \to |N + R\rangle) = \left\{ \left(\prod_{n \in N} \beta_n \right) \left(\prod_{i \in I} \sqrt{1 - e^{-2f_i}} \sum_{V_i} c_{V_i}^2 e^{-F_{V_i}} \right) \left(\prod_{a \in A} \sum_{V_a} c_{V_a}^2 e^{-F_a - F_{V_a}} \right) \right\}$$

$$\times \left\{ \left(\prod_{r \in R} \beta_r \alpha_r \right) \left(\prod_{p \in P} \sum_{V_p} c_{V_p}^2 e^{-F_p - F_{V_p}} \right) \left(\prod_{l \in L} \sum_{V_l} c_{V_l}^2 (1 - e^{-F_l - F_{V_l}}) \right) \right\} \quad \text{(B.4)}$$

This result can be implemented in a future version of DIPSY, and would imply slightly higher multiplicities in non-diffractive events.

References

[1] **H1** Collaboration, C. Adloff *et al.*, *Z.Phys.* **C76** (1997) 613–629, `arXiv:hep-ex/9708016` `[hep-ex]`.

[2] **ZEUS** Collaboration, S. Chekanov *et al.*, *Nucl.Phys.* **B713** (2005) 3–80, `arXiv:hep-ex/0501060 [hep-ex]`.

[3] **UA4** Collaboration, D. Bernard *et al.*, *Phys.Lett.* **B166** (1986) 459.

[4] **UA5** Collaboration, R. E. Ansorge *et al.*, *Z. Phys.* **C33** (1986) 175.

[5] **CDF** Collaboration, F. Abe *et al.*, *Phys. Rev.* **D50** (1994) 5535–5549.

[6] A. H. Mueller, *Phys. Rev.* **D2** (1970) 2963–2968.

[7] C. E. DeTar *et al.*, *Phys. Rev. Lett.* **26** (1971) 675–676.

[8] V. Abramovsky, V. Gribov, and O. Kancheli, *Yad.Fiz.* **18** (1973) 595–616.

[9] A. Kaidalov and M. Poghosyan, *Eur.Phys.J.* **C67** (2010) 397–404, `arXiv:0910.2050` `[hep-ph]`.

[10] S. Ostapchenko, *Phys.Rev.* **D83** (2011) 014018, `arXiv:1010.1869 [hep-ph]`.

[11] M. Ryskin, A. Martin, and V. Khoze, *Eur.Phys.J.* **C71** (2011) 1617, `arXiv:1102.2844` `[hep-ph]`.

[12] M. Ryskin, A. Martin, and V. Khoze, *Eur.Phys.J.* **C72** (2012) 1937, `arXiv:1201.6298` `[hep-ph]`.

[13] E. Gotsman, A. Kormilitzin, E. Levin, and U. Maor, *Nucl.Phys.* **A842** (2010) 82–101, `arXiv:0912.4689` `[hep-ph]`.

[14] E. Gotsman, E. Levin, and U. Maor, *Phys.Rev.* **D85** (2012) 094007, `arXiv:1203.2419` `[hep-ph]`.

[15] E. Gotsman, E. Levin, and U. Maor, `arXiv:1208.0898` `[hep-ph]`.

[16] A. Martin, H. Hoeth, V. Khoze, F. Krauss, M. Ryskin, *et al.*, `arXiv:1206.2124` `[hep-ph]`.

[17] M. L. Good and W. D. Walker, *Phys. Rev.* **120** (1960) 1857–1860.

[18] H. I. Miettinen and J. Pumplin, *Phys. Rev.* **D18** (1978) 1696.

[19] A. H. Mueller, *Nucl.Phys.* **B335** (1990) 115.

[20] Y. Hatta, E. Iancu, C. Marquet, G. Soyez, and D. Triantafyllopoulos, *Nucl.Phys.* **A773** (2006) 95–155, `arXiv:hep-ph/0601150` `[hep-ph]`.

[21] E. Avsar, G. Gustafson, and L. Lönnblad, *JHEP* **12** (2007) 012, `arXiv:0709.1368` `[hep-ph]`.

[22] C. Flensburg and G. Gustafson, *JHEP* **1010** (2010) 014, `arXiv:1004.5502` `[hep-ph]`.

[23] G. Gustafson, `arXiv:1206.1733` `[hep-ph]`.

[24] A. Edin, G. Ingelman, and J. Rathsman, *Phys.Lett.* **B366** (1996) 371–378, `arXiv:hep-ph/9508386` `[hep-ph]`.

[25] R. Pasechnik, R. Enberg, and G. Ingelman, *Phys.Lett.* **B695** (2011) 189–193, `arXiv:1004.2912` `[hep-ph]`.

[26] K. J. Golec-Biernat and M. Wusthoff, *Phys.Rev.* **D60** (1999) 114023, `arXiv:hep-ph/9903358` `[hep-ph]`.

[27] K. J. Golec-Biernat and M. Wusthoff, *Eur. Phys. J.* **C20** (2001) 313–321, `arXiv:hep-ph/0102093`.

[28] K. Goulianos, *Phys. Lett.* **B358** (1995) 379–388, `arXiv:hep-ph/9502356`.

[29] **EHS/NA22** Collaboration, M. Adamus *et al.*, *Z.Phys.* **C39** (1988) 301.

[30] **R608** Collaboration, A. Smith *et al.*, *Phys.Lett.* **B163** (1985) 267.

[31] **R608** Collaboration, A. Smith *et al.*, *Phys.Lett.* **B167** (1986) 248.

[32] A. Donnachie and P. Landshoff, *Nucl.Phys.* **B244** (1984) 322.

[33] **H1** Collaboration, C. Adloff *et al.*, *Eur.Phys.J.* **C1** (1998) 495–507, `arXiv:hep-ex/9711006` `[hep-ex]`.

[34] **UA8** Collaboration, R. Bonino *et al.*, *Phys. Lett.* **B211** (1988) 239.

[35] **CDF** Collaboration, T. Affolder *et al.*, *Phys.Rev.Lett.* **84** (2000) 5043–5048.

[36] **D0** Collaboration, B. Abbott *et al.*, *Phys.Lett.* **B531** (2002) 52–60, `arXiv:hep-ex/9912061` `[hep-ex]`. 11 pages 4 figures. submitted to PRL Report-no: Fermilab PUB-99/375-E.

[37] **ZEUS** Collaboration, S. Chekanov *et al.*, *Eur.Phys.J.* **C52** (2007) 813–832, `arXiv:0708.1415 [hep-ex]`.

[38] **H1** Collaboration, F. Aaron *et al.*, `arXiv:1111.0584 [hep-ex]`. Long author list - awaiting processing.

[39] **CDF** Collaboration, T. Aaltonen *et al.*, *Phys.Rev.* **D77** (2008) 052004, `arXiv:0712.0604 [hep-ex]`.

[40] **CDF** Collaboration, A. Abulencia *et al.*, *Phys.Rev.Lett.* **98** (2007) 112001, `arXiv:hep-ex/0611040 [hep-ex]`.

[41] G. Ingelman and P. E. Schlein, *Phys. Lett.* **B152** (1985) 256.

[42] **ZEUS** Collaboration, S. Chekanov *et al.*, *Nucl.Phys.* **B831** (2010) 1–25, `arXiv:0911.4119 [hep-ex]`.

[43] P. Bruni, A. Edin, and G. Ingelman, "POMPYT version 2.6." Unpublished.

[44] H. Jung, *Comput.Phys.Commun.* **86** (1995) 147–161.

[45] T. Sjöstrand, S. Mrenna, and P. Skands, *Comput. Phys. Commun.* **178** (2008) 852–867, `arXiv:0710.3820 [hep-ph]`.

[46] E. Avsar, G. Gustafson, and L. Lönnblad, *JHEP* **07** (2005) 062, `hep-ph/0503181`.

[47] C. Flensburg, G. Gustafson, and L. Lönnblad, *JHEP* **1108** (2011) 103, `arXiv:1103.4321 [hep-ph]`.

[48] R. Glauber, , in *Lectures in Theoretical Physics*, W. Brittin and L. Dunham, eds., vol. I, p. 315. Interscience Publishers, Inc., New York, 1957.

[49] A. H. Mueller, *Nucl. Phys.* **B415** (1994) 373–385.

[50] A. H. Mueller and B. Patel, *Nucl. Phys.* **B425** (1994) 471–488, `hep-ph/9403256`.

[51] A. H. Mueller, *Nucl. Phys.* **B437** (1995) 107–126, `hep-ph/9408245`.

[52] E. Avsar, G. Gustafson, and L. Lönnblad, *JHEP* **01** (2007) 012, `hep-ph/0610157`.

[53] C. Flensburg, G. Gustafson, and L. Lönnblad, *Eur. Phys. J.* **C60** (2009) 233–247, `arXiv:0807.0325 [hep-ph]`.

[54] G. P. Salam, *Acta Phys. Polon.* **B30** (1999) 3679–3705, `hep-ph/9910492`.

[55] J. Kwiecinski, A. D. Martin, and P. J. Sutton, *Z. Phys.* **C71** (1996) 585–594, `hep-ph/9602320`.

[56] I. Balitsky and G. A. Chirilli, *Acta Phys.Polon.* **B39** (2008) 2561–2566.

[57] E. Avsar, *JHEP* **04** (2008) 033, `arXiv:0803.0446 [hep-ph]`.

[58] S. Catani, F. Fiorani, and G. Marchesini, *Nucl. Phys.* **B336** (1990) 18.

[59] M. Ciafaloni, *Nucl. Phys.* **B296** (1988) 49.

[60] B. Andersson, G. Gustafson, and J. Samuelsson, *Nucl. Phys.* **B467** (1996) 443–478.

[61] G. Salam, *JHEP* **9903** (1999) 009, `arXiv:hep-ph/9902324 [hep-ph]`.

[62] G. Gustafson and G. Miu, *Phys.Rev.* **D63** (2001) 034004, `arXiv:hep-ph/0002278 [hep-ph]`.

[63] M. Bähr *et al.*, *Eur. Phys. J.* **C58** (2008) 639–707, `arXiv:0803.0883 [hep-ph]`.

[64] G. Gustafson, *Phys. Lett.* **B175** (1986) 453.

[65] G. Gustafson and U. Pettersson, *Nucl. Phys.* **B306** (1988) 746.

[66] L. Lönnblad, *Comput. Phys. Commun.* **71** (1992) 15–31.

[67] B. Andersson, G. Gustafson, and B. Söderberg, *Z. Phys.* **C20** (1983) 317.

[68] B. Andersson, G. Gustafson, G. Ingelman, and T. Sjöstrand, *Phys. Rept.* **97** (1983) 31.

[69] T. Sjöstrand, S. Mrenna, and P. Skands, *JHEP* **05** (2006) 026, `arXiv:hep-ph/0603175`.

[70] **H1** Collaboration, C. Adloff *et al.*, *Eur.Phys.J.* **C5** (1998) 439–452, `arXiv:hep-ex/9804012`
    `[hep-ex]`.

[71] **H1** Collaboration, C. Adloff *et al.*, *Phys.Lett.* **B428** (1998) 206–220, `arXiv:hep-ex/9803032`
    `[hep-ex]`.